UNIVERSITÀ DEGLI STUDI
DI NAPOLI FEDERICO II

Erfan Noferesti

Performance of RC beams strengthened with inorganic composite materials

FRP++
Advanced structural analysis and
design using composite materials

Master Dissertation
European Master Advanced Structural Analysis and
Design using Composite Materials

Work developed under the supervision of
Professor Marta Del Zoppo
Professor Marco Di Ludovico

Funded by
the European Union

September 2025

DECLARATION

Name: Erfan Noferesti

Email: erfanof589@gmail.com **Phone number:** +393445216972

Title of the Thesis: Performance of RC beams strengthened with inorganic composite materials

Supervisors:

Professor Marta Del Zoppo

Professor Marco Di Ludovico

Year of Conclusion: 2025

Master Course in Advanced Structural Analysis and Design using Composite Materials

University of Naples Federico II, 09/04/2025

Signature:

ACKNOWLEDGEMENTS

First and foremost, I would like to express my deepest gratitude to my parents, whose unwavering love, support, and encouragement have been the foundation of all my achievements. Their belief in me has been my greatest strength throughout this journey.

I am profoundly thankful to Professor Marta Del Zoppo, my supervisor, for her invaluable guidance, constructive feedback, and continuous encouragement throughout this thesis. Her expertise and mentorship have deeply shaped my academic path. I also extend my appreciation to Professor Marco Di Ludovico, whose insights and support added great value to my research.

A special thanks goes to Mikias Fekadeselassie Mekbebe, whose generous help, clarity of thought, and constant willingness to assist were instrumental in my understanding and progression of this work. I truly appreciated his patience and academic support.

I am also grateful to all my colleagues, whose camaraderie and intellectual discussions made this experience rich and fulfilling. A heartfelt thank you to my friends, both in Italy and Iran and rest of the world, who stood by me through the ups and downs, bringing moments of joy, relief, and motivation.

My sincere appreciation goes to Professor Christina Barris from the University of Girona, whose teaching and dedication to materials science left a lasting impression on me and influenced this work more than she might realize.

To all the staff at UNINA, I am thankful for the supportive and professional environment you provided during my studies. In particular, I am indebted to Valeria, whose kindness, efficiency, and unwavering help made many things smoother behind the scenes.

Finally, I would like to acknowledge the FRP++ Erasmus Mundus Program and its coordinators for providing me with this unique academic opportunity and the enriching international experience it entailed. Their commitment to excellence and support throughout the program have been crucial to my academic growth and personal development.

To everyone mentioned here, and to those who were a part of this journey in big or small ways—thank you from the bottom of my heart.

Comportamento di travi in calcestruzzo armato rinforzate con materiali compositi inorganici

RIASSUNTO

Il deterioramento delle strutture in calcestruzzo armato (RC) invecchiate, la crescente domanda di rinforzo flessionale dovuta al cambio di destinazione d'uso degli edifici, alle azioni sismiche e all'aggiornamento delle normative di progettazione hanno intensificato la necessità di tecniche di rinforzo efficaci e durevoli per la capacità flessionale. I metodi tradizionali di rinforzo spesso risultano carenti in termini di duttilità, compatibilità e prestazioni a lungo termine. In questo contesto, l'impiego dei compositi cementizi fibrorinforzati inorganici (FRCC) è emerso come una valida alternativa, offrendo un comportamento meccanico migliorato, una maggiore sostenibilità ambientale e una migliore compatibilità con gli elementi in calcestruzzo esistenti.

La presente tesi indaga le prestazioni strutturali di travi in calcestruzzo armato rinforzate con sistemi ibridi FRCC composti da fibre di acciaio riciclato e fibre di polietilene (PE). Sono state studiate due configurazioni di rinforzo: rinforzo inferiore e a "U-jacketing". La ricerca prende avvio dalla caratterizzazione del materiale attraverso prove di flessione a tre punti e prove di compressione, seguite da prove di flessione a quattro punti su provini di travi rinforzate, al fine di valutare il comportamento flessionale, i quadri fessurativi e le modalità di rottura.

Per la valutazione dello sviluppo delle fessure durante il carico è stata impiegata la tecnica della Digital Image Correlation (DIC), che ha consentito di acquisire dati di deformazione a campo pieno. Inoltre, è stato sviluppato e calibrato un modello agli elementi finiti sulla base dei risultati sperimentali per valutare le proprietà del materiale e il comportamento delle travi. È stato inoltre condotto uno studio parametrico per analizzare l'influenza della resistenza a trazione del FRCC, della resistenza a compressione del calcestruzzo e del diametro dell'armatura longitudinale sulla risposta strutturale di travi in calcestruzzo armato a scala reale.

I risultati hanno confermato che entrambi i metodi di rinforzo con FRCC sono in grado di fornire un incremento della capacità flessionale fino al 40% e di migliorare il comportamento post-fessurativo delle travi. In particolare, il rinforzo a U-jacketing ha determinato una maggiore distribuzione delle fessure, una capacità di deformazione superiore e una migliore stabilità nella fase post-picco. Questi risultati dimostrano l'efficacia dei sistemi FRCC a base di acciaio per il rinforzo strutturale e ne evidenziano il potenziale come soluzione sostenibile e ad alte prestazioni per il miglioramento delle strutture in calcestruzzo armato esistenti.

PAROLE CHIAVE: FRCC; U-jacketing e rinforzo inferiore; Flessione a quattro punti; Fibre di acciaio; ABAQUS; DIC.

Performance of RC beams strengthened with inorganic composite materials

ABSTRACT

The deterioration of aging reinforced concrete (RC) structures, the increasing demand for flexural strengthening due to the change of use in buildings, seismic actions and updated design codes have intensified the need for effective and durable strengthening techniques for flexural capacity. Traditional retrofitting methods often fall short in terms of ductility, compatibility, and long-term performance. In this context, the use of inorganic fiber-reinforced cementitious composites (FRCC) has emerged as a promising alternative, offering improved mechanical behavior, environmental sustainability, and compatibility with existing concrete members.

This thesis investigates the structural performance of RC beams strengthened with hybrid FRCC systems composed of recycled steel fibers and polyethylene (PE) fibers. Two strengthening configurations are studied: bottom reinforcement and U-jacketing. The research begins with material characterization through three-point bending and compression tests, followed by four-point bending tests on retrofitted beam specimens to evaluate flexural behavior, crack patterns, and failure modes.

Digital Image Correlation (DIC) was employed to capture full-field strain data and analyze crack development under loading. Additionally, a finite element model was developed and calibrated using the experimental results in order to evaluate the material properties and behavior of the beams. Moreover, a parametric study was performed to evaluate the influence of FRCC tensile strength, concrete compressive strength, and longitudinal reinforcement diameter on the structural response of real scale RC beams.

The results confirmed that both FRCC strengthening methods are bale to provide an increase in flexural capacity up to 40% and improve the post-cracking behavior of the beams. U-jacketing, in particular, resulted in more distributed cracking, higher deformation capacity, and improved stability during the post-peak phase. These findings demonstrate the effectiveness of steel-FRCC systems for structural retrofitting and highlight their promise as a sustainable and high-performance solution for enhancing existing RC structures.

KEYWORDS: FRCC; U-jacketing and bottom reinforcement; Four point bending; Steel fibers; ABAQUS; DIC.

TABLE OF CONTENTS

LIST OF FIGURES

LIST OF TABLES

List of Abbreviations and Symbols

Abbreviations

AFRP	Aramid Fiber Reinforced Polymer
BFRP	Basalt Fiber Reinforced Polymer
CFRP	Carbon Fiber Reinforced Polymer
DIC	Digital Image Correlation
EBR	Externally Bonded Reinforcement
ECC	Engineered Cementitious Composite
FEM	Finite Element Method / Modelling
FRCC	Fiber Reinforced Cementitious Composite
FRP	Fiber Reinforced Polymer
FRCM	Fabric-Reinforced Cementitious Matrix
GFRP	Glass Fiber Reinforced Polymer
ITZ	Interfacial Transition Zone
LCA	Life Cycle Assessment
LVDT	Linear Variable Displacement Transducer
NSM	Near Surface Mounted
PE	Polyethylene
RC	Reinforced Concrete
RFAC	Recycled Fine Aggregate Concrete
SMA	Shape Memory Alloy
TR-SHGC	Textile-Reinforced Strain-Hardening Geopolymer Composite

Symbols

E_f	Elastic modulus of the CFRP laminate
ε_f	Ultimate strain of the CFRP laminate
f_{ck}	Characteristic compressive strength of concrete
f_{cm}	Mean compressive strength of concrete
E_c	Elastic modulus of concrete
ρ	Density (for both concrete and steel, depending on context)

f_{yk}	Characteristic yield strength of reinforcement steel
f_{uk}	Characteristic ultimate strength of reinforcement steel
ε_{yk}	Characteristic yield strain of reinforcement steel
ε_{uk}	Characteristic ultimate strain of reinforcement steel
E_s	Elastic modulus of reinforcement steel
ε	Strain
σ	Stress
τ	Shear stress
θ	Dilation Angle

THIS PAGE WAS INTENTIONALLY LEFT BLANK

1. INTRODUCTION

The continuous aging of reinforced concrete (RC) infrastructure and the increasing frequency and intensity of seismic events around the world have amplified the urgency for effective and sustainable structural strengthening solutions[1]. Many existing RC buildings and bridges were designed according to outdated codes and lack the ductility and energy dissipation capacity necessary to withstand modern seismic demands. As retrofitting and upgrading these structures becomes more critical, the development and application of advanced materials play a pivotal role in ensuring public safety, reducing economic losses, and extending the service life of built assets.

Among the available retrofit technologies, the use of composite materials has gained widespread attention due to their high strength-to-weight ratio, ease of application, and excellent durability. Traditionally, fiber-reinforced polymer (FRP) composites bonded with organic resins such as epoxy have been employed for strengthening RC elements. However, these materials present several limitations under extreme environmental and mechanical conditions, including poor fire resistance, susceptibility to ultraviolet degradation, and limited performance at elevated temperatures—conditions often encountered during and after seismic events[2].

To overcome these challenges, inorganic composite materials, particularly Fiber-Reinforced Cementitious Composites (FRCCs), have emerged as a promising alternative. FRCCs are a class of high-performance materials characterized by a cement-based matrix embedded with discontinuous fibers. In this research, steel fibers are employed as the reinforcing phase within the cementitious matrix. The incorporation of steel fibers distinguishes this system from conventional FRP composites that typically use glass or carbon fibers embedded in the resin[3].

The use of steel fibers in FRCCs brings several critical advantages, particularly in the context of seismic strengthening. First, steel fibers exhibit superior ductility and toughness, which are essential for energy dissipation under cyclic loading. Unlike glass or carbon fibers, which are brittle and prone to sudden rupture, steel fibers can undergo significant plastic deformation, thereby enhancing the post-cracking behavior of the composite. This ductile response is critical in maintaining the integrity and load-carrying capacity of RC members during seismic events[4].

Second, steel fibers offer better bond performance with the cementitious matrix due to their mechanical anchorage and surface roughness, reducing the likelihood of fiber pull-out under high strain rates. This enhances the composite's ability to distribute stresses and control crack widths more effectively than traditional FRPs. Additionally, steel fibers are thermally stable, providing superior fire resistance compared to glass or carbon fibers bound in polymer matrices, which may degrade or combust at elevated temperatures[5].

Moreover, steel-fiber-reinforced systems are inherently compatible with existing concrete in terms of thermal expansion, modulus of elasticity, and chemical composition. This compatibility reduces the risk of interface debonding or differential movement, further improving the long-term durability and reliability of the strengthening system under both static and dynamic loading[6]. Furthermore, one of the most compelling advantages of FRCCs in seismic strengthening lies in their enhanced ductility and crack control capabilities. Unlike traditional strengthening techniques, which may lead to brittle failure modes or localized stress concentrations, FRCCs contribute to a more distributed cracking pattern and improve post-yield behavior of structural members. This results in enhanced deformation capacity, increased energy dissipation, and delayed onset of failure—key performance indicators during seismic events[7].

For this matter, several structural strengthening strategies have been developed and implemented, each with distinct mechanisms and levels of effectiveness. The selection of a suitable technique often depends on factors such as structural accessibility, performance objectives, construction constraints, and the specific deficiencies of the member. Among the commonly adopted methods in seismic retrofitting are U-jacketing and bottom reinforcement retrofitting, both of which can be effectively integrated with advanced composite materials such as steel-FRCCs[8], [9].

U-jacketing is a widely used technique for enhancing the flexural and shear capacity of RC beams, especially in regions where full wrapping is impractical due to floor slab constraints. In this method, the composite material such as steel-FRCC is applied in a U-shaped configuration around the three accessible faces of the beam (two vertical sides and the soffit). This jacket acts as an external reinforcement, improving confinement, delaying crack propagation, and enhancing the load-bearing capacity. When used with a ductile and crack-controlling material like FRCC, the U-jacketing not only strengthens the section but also enhances energy dissipation during cyclic loading, making it highly effective against seismic actions. Moreover, the cementitious nature of the FRCC ensures compatibility with the existing concrete surface, promoting better adhesion and durability over time[10].

In contrast, the bottom reinforcement method is a more intrusive but highly targeted technique, particularly suitable for addressing deficiencies in flexural capacity. In this method, the bottom cover or a segment of the tension zone of the beam is selectively removed to expose the internal reinforcement or to create space for placing new high-performance strengthening layers. After surface preparation, steel-FRCC layers are cast directly onto the newly exposed surface, bonding monolithically with the original structure. This approach allows the new material to work integrally with the original beam, directly counteracting tensile stresses that dominate during bending under seismic loads[11]. Both shapes are shown in figure1.1.

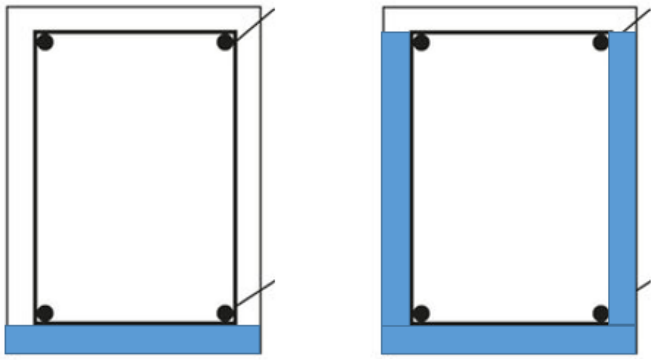

(a) Bottom Reinforcement (b) U Jacketing

Figure 2.1 Strengthening Shapes

The advantage of the bottom reinforcement approach lies in its ability to maximize mechanical interlock and stress transfer efficiency, particularly when the strengthening layer is strategically placed within the most critical tension region. Combined with the high ductility, strain-hardening behavior, and crack-bridging capacity of steel-FRCCs, this method significantly enhances the flexural performance and post-yield behavior of the beam. Additionally, it minimizes the risk of debonding or delamination that may occur in externally bonded solutions under repeated seismic loading[11].

1.1. Motivation

In regions where current structure does not demonstrates enough flexural capacity due to change in use, recurring seismic activity or updated design codes, the long-term performance of retrofitted structures-not just their immediate post-event response-has become a key concern for infrastructure resilience planning. Yet, most strengthening systems are evaluated in terms of ultimate capacity, with limited insight into their residual performance, reparability, and integration into life-cycle design strategies.

Steel-FRCCs offer a unique opportunity in this context. Their distributed cracking behavior, energy dissipation capacity, and crack bridging mechanisms suggest the potential for damage-tolerant designs, which could reduce repair demands and downtime. However, current literature lacks performance metrics tailored to such criteria, especially when FRCCs are applied as structural interventions through U-jacketing or bottom reinforcement. This motivates a broader investigation into FRCC strengthening techniques for increasing the flexural capacity of the retrofitted structures. Also, distinct fibers used in this material and the effectiveness of the fiber ratio is a crucial subject which needs to be studied in depth in order to understand the behaviour of the FRCC material.

Additionally, while this material offers promising properties and behaviour, there is no standard or design codes as a reference. Furthermore, the lack of enough validations of this material in the current literature, resulted in more necessity in FRCC analysis.

1.2. Objectives

This dissertation investigates the performance of RC beams retrofitted with steel-FRCCs, focusing on their flexural capacity. Through experimental testing and analytical modeling, the research aims to assess the improvements in flexural strength, ductility, and energy absorption provided by different FRCC systems. By comparing the retrofitted performance with unstrengthen counterparts, the study provides insights into the mechanisms by which steel-FRCCs enhance flexural capacity, and identifies the parameters that govern their effectiveness.

Moreover, the findings contribute to the ongoing effort to establish robust, sustainable, and resilient retrofitting strategies for RC structures. The integration of steel-FRCCs into practical engineering solutions holds the potential not only to reduce seismic vulnerability but also to support the transition toward greener and more durable infrastructure systems.

Furthermore, a parametric analysis is implemented for distinct FRCC tensile capacities, various concrete grades and several diameters of tensile longitudinal reinforcement. This practice widen the perspective in the primary affecting parameters of RC beams strengthened with FRCC material. Also, due to the actual sizing (full scale beam with real structure sizing) used in this analysis, it suggests a robust simulation for practical cases.

1.3. Structure of the Dissertation

This thesis is structured into five chapters. Chapter 1 introduces the background and motivation for the study, outlines the key research questions and objectives, and presents the structure of the work. Chapter 2 provides a concise literature review on the seismic strengthening of reinforced concrete structures, discussing conventional and advanced strengthening techniques. It also includes a general overview of fiber-reinforced polymers (FRP) and fiber-reinforced cementitious composites (FRCC), covering their mechanical characteristics, advantages, and application potential in structural retrofitting. Chapter 3 details the experimental testing, including material characterization and beam flexural testing with four point bending to evaluate the structural performance of strengthened elements. Chapter 4 presents the numerical modelling of the beams, incorporating both material and structural simulations, and concludes with a parametric study on the behavior of full-scale beams under various strengthening configurations. Finally, Chapter 5 discusses the key findings, and concludes with reflections on the study's contributions and suggestions for future research.

THIS PAGE WAS INTENTIONALLY LEFT BLANK

2. LITERATURE REVIEW

2.1. Strengthening for Flexural Loading

Flexural strengthening is pursued when existing structural members—most commonly reinforced concrete (RC) beams and slabs—no longer provide adequate bending resistance relative to current performance requirements. In practice, insufficient flexural capacity manifests as excessive deflection, wide tensile cracking, reduced stiffness, and limited ductility, all of which compromise safety and serviceability. The need to upgrade flexural performance typically arises from three dominant drivers: change of use, evolution of design codes, and seismic actions. Across these contexts, the objective is to increase ultimate moment capacity and deformation capacity while controlling service-level responses (deflection and crack width), often with minimal interruption to building operations.

2.1.1. Change of Use

When a structure undergoes a change of use, its original design assumptions regarding applied loads, functional requirements, and service conditions are no longer valid. Most buildings are designed for a specific purpose, such as residential occupancy, office use, or storage, each of which corresponds to a prescribed set of dead and live loads defined by design codes[12]. When the use of the structure changes—for instance, when a residential building is converted into an office, a warehouse, or a laboratory—the imposed loads can increase significantly. Offices and laboratories often demand higher live loads due to greater occupant density, heavier equipment, or specialized installations. Similarly, the introduction of storage areas, archives, or mechanical facilities may add large concentrated loads or continuous distributed loads that were not accounted for in the initial design. This increase in loading elevates the bending moments and shear forces experienced by beams and slabs, leading to excessive flexural demand relative to their original capacity[13].

Beyond loading changes, aging effects play a key role in reducing the inherent capacity of the structure at the time of functional transformation. Over time, reinforced concrete members may suffer from steel corrosion, concrete cracking, loss of bond between reinforcement and concrete, and general material degradation due to environmental exposure[14]. These effects reduce the effective cross-sectional properties and stiffness of structural members, compromising their ability to resist flexural stresses.

Consequently, when a building is repurposed, the combination of higher applied demands and lower residual capacity makes strengthening necessary to ensure safety and serviceability[15].

Flexural strengthening in such cases aims to restore and enhance the bending resistance of critical members. Externally bonded reinforcement systems using fiber-reinforced polymers (FRP) are often adopted due to their high strength-to-weight ratio, ease of application, and minimal added dead load. Alternatively, near-surface mounted (NSM) reinforcement, steel plate bonding, or inorganic overlays with fiber-reinforced cementitious composites (FRCC) can be employed to provide additional tensile capacity and improve crack control. These techniques not only increase ultimate flexural strength but also help to control deflection and limit serviceability issues under sustained loading. Proper attention to anchorage, bond quality, and compatibility with the existing substrate is essential to ensure effective performance[16].

2.1.2. Updated Design Codes

The continuous evolution of structural design codes and assessment standards has created an additional and important motivation for flexural strengthening. Many existing structures, particularly those constructed in the mid to late twentieth century, were designed according to codes that differ substantially from present-day requirements[17]. Modern codes incorporate more comprehensive and realistic load models, higher safety and importance factors, stricter durability provisions, and explicit checks for serviceability and robustness. When older structures are reassessed using these updated criteria, deficiencies in flexural capacity often become evident. Typical shortcomings include inadequate longitudinal reinforcement ratios, inefficient bar arrangements, and limited effective depth, which may compromise the member's ability to resist current design bending moments.

To address these deficiencies revealed by modern design codes, strengthening interventions are typically directed towards achieving measurable improvements in flexural resistance, stiffness, and ductility, while ensuring compliance with updated detailing provisions. The primary goal is to restore or enhance the load-carrying capacity of members so that they can safely sustain the revised design bending moments and service-level demands. Achieving this objective requires not only an increase in the ultimate moment strength but also adequate control of deflections, crack widths, and overall deformation capacity[18], [19].

The choice of strengthening method is often governed by a balance between structural efficiency, constructability, and long-term durability. In practice, interventions may take the form of externally applied reinforcements, overlays, or section enlargements, each aiming to provide additional tensile capacity and to optimize the stress distribution across the section[20]. Regardless of the technique, special attention

must be given to the transfer of stresses between the existing substrate and the added material, since bond performance and anchorage detailing largely determine the effectiveness of the strengthening system. Premature failures—such as debonding, anchorage slip, or local crushing—can undermine the expected gains, making detailing and quality control critical aspects of implementation[21].

2.1.3. Strengthening For Seismic Actions

Seismic events pose a significant threat to the safety and serviceability of existing reinforced concrete (RC) structures, especially those designed before the enforcement of modern seismic design codes. Many older buildings exhibit vulnerabilities such as inadequate reinforcement detailing, insufficient ductility, poor confinement in plastic hinge regions, and inadequate lap splice lengths. These shortcomings often result in brittle failure modes under seismic loading, leading to structural collapse which is shown in figure2.1. The need for strengthening such buildings against seismic actions has driven extensive research and development of both traditional and advanced retrofitting techniques, with the goal of enhancing structural resilience during earthquakes[22].

Figure 2.1 Column failure due to seismic actions

In response to these deficiencies, structural engineers have developed a wide range of strengthening techniques to rehabilitate and improve the performance of aging RC structures. Strengthening not only aims to restore or enhance the original capacity of the structure but also to meet updated performance objectives, extend the service life, and ensure the safety of occupants and surrounding infrastructure.

The process of strengthening existing RC structures follows a methodical and engineering-driven approach that begins with a thorough understanding of the structure's current condition. Initially, a preliminary assessment is carried out, involving a detailed review of available architectural and structural drawings, past maintenance records, and previous retrofit interventions. This is followed by a visual inspection to

identify obvious signs of structural distress such as cracking, spalling, deformation, corrosion stains, and water ingress[23].

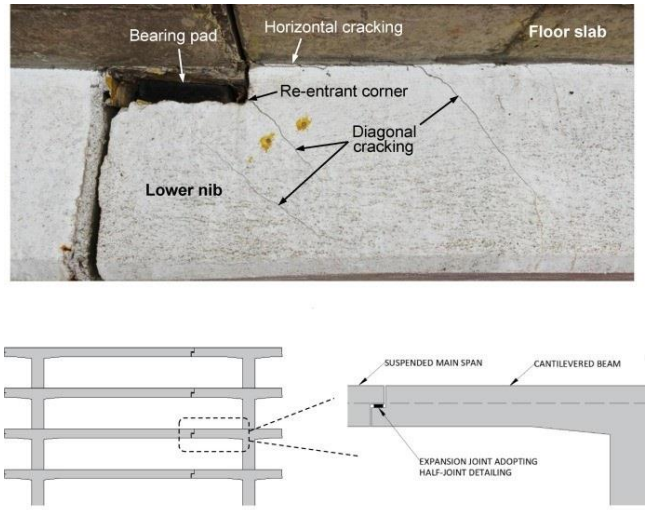

Figure 2.2 Visual inspection of structures showing early signs of distress

In many cases, surface-level observations are insufficient to assess the true extent of deterioration or internal damage. Therefore, the next stage involves more detailed and often intrusive inspections using both non-destructive and destructive testing techniques. Non-destructive testing (NDT) methods such as ultrasonic pulse velocity, rebound hammer, ground penetrating radar, and half-cell potential testing are employed to evaluate material uniformity, locate reinforcement, and assess corrosion activity[23].

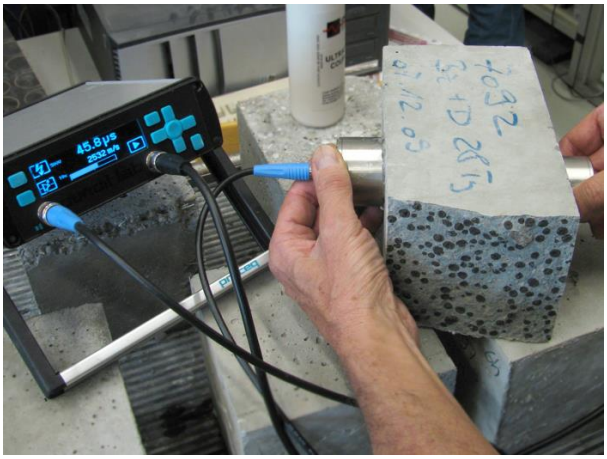

Figure 2.3 ultrasonic pulse velocity testing to assess internal integrity of concrete

Following the condition assessment, a comprehensive structural evaluation is conducted to analyze the existing load-carrying capacity of the structure under current and projected loads. This involves developing analytical or numerical models based on actual geometry, material properties, and reinforcement

detailing. Finite element analysis or other suitable structural analysis methods are used to simulate various loading scenarios, including gravity loads, wind loads, and seismic actions.

Once the critical vulnerabilities are identified, a suitable strengthening strategy is formulated. One widely used technique is section enlargement or jacketing, where additional concrete, steel, or fiber-reinforced cementitious composite (FRCC) material is added around beams, columns, or slabs to increase their cross-sectional area and improve strength and stiffness. Concrete jacketing involves placing additional reinforced concrete around an existing member with adequate surface preparation and bonding[24].

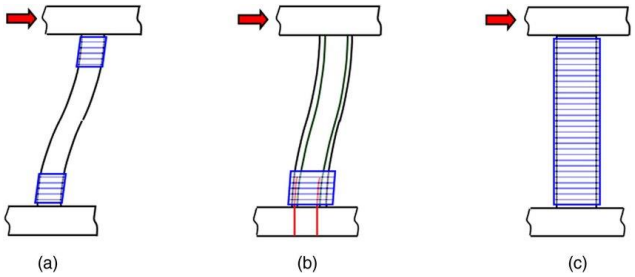

Figure 2.4 RC column being retrofitted using jacketing to improve confinement and load capacity

In some cases, strengthening requires the addition of new structural elements such as concrete shear walls, steel braces, or new frames to increase lateral stiffness and load redistribution. In situations where the existing foundations are inadequate, foundation interventions such as underpinning, micro-piling, or footing enlargement may be necessary[25].

The implementation of strengthening measures must be carried out with precision and adherence to detailed specifications. Surface preparation is critical to ensure proper bonding between the new and existing materials. Once the materials are installed, structural health monitoring systems, such as strain gauges, displacement sensors, and crack monitors, may be integrated to evaluate performance over time.

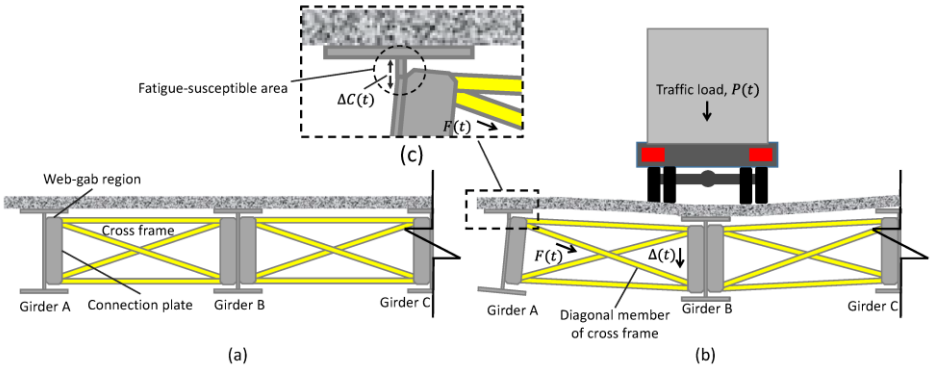

Figure 2.5 structural health monitoring systems

Strengthening of existing RC structures demands a nuanced and context-specific approach that integrates structural assessment, advanced materials, and carefully selected retrofitting techniques. Whether through traditional methods like concrete jacketing or innovative solutions such as externally bonded

FRPs, near-surface mounted reinforcements, or fiber-reinforced cementitious composites, the goal remains the same: to restore or enhance the structural capacity, ductility, and durability of deficient elements. The combination of thorough diagnostics, analytical modeling, and modern material systems enables engineers to tailor strengthening strategies that not only address current performance gaps but also prepare the structure for future demands, including seismic resilience and extended service life.

2.2. Traditional Strengthening Techniques

The retrofitting of reinforced concrete (RC) structures involves a wide array of strengthening techniques tailored to address various structural deficiencies such as inadequate flexural strength, insufficient shear resistance, low ductility, or poor serviceability. These techniques fall into traditional or advanced categories and are selected based on the type of structural deficiency, accessibility, cost constraints, and particularly the expected seismic performance[26].

2.2.1. Concrete Jacketing

Concrete jacketing is one of the oldest strengthening methods used to increase the cross-sectional area and reinforcement content of existing structural members, especially columns. This method typically involves casting a new layer of concrete with added reinforcement around the existing member. It enhances axial, shear, and bending capacity and significantly improves confinement and ductility under seismic loading. However, it also increases the dead load and requires thorough surface preparation to ensure proper action between old and new concrete[27]. Figure 1 shows a typical concrete jacketing application around a column.

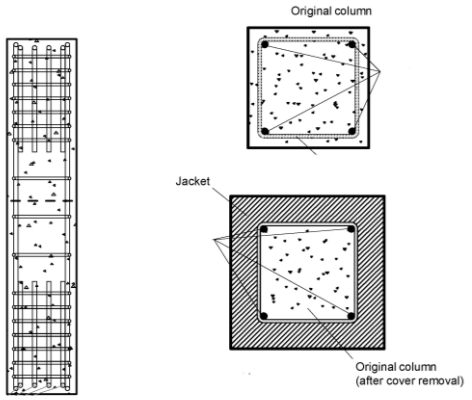

Figure 2.6 Concrete jacketing of an RC column

2.2.2. Steel Jacketing

Steel jacketing is another conventional technique used to encase RC columns or beams with steel plates or angles, which are either bolted or welded. It improves shear capacity and provides lateral confinement. This method is effective for rapid retrofitting, especially in seismic zones. However, the major drawbacks include corrosion susceptibility of steel and the need for protective coatings, as well as the complex labor involved in welding or bolting steel components[28].

Figure 2.7 Steel jacketing of a column

2.2.3. Post-Tensioning

Post-tensioning introduces external forces into the structure by applying tensioned steel tendons. This method reduces deflection, enhances crack control, and increases overall strength. It is typically used in long-span structures like bridges or floor slabs. The process is labor-intensive and must be executed with precision, especially for anchorage and tensioning systems[29].

Figure 2.8 Applied Post-tensioning cables

2.3. Fiber Reinforced Polymer (FRP)

2.3.1. Introduction

Fiber-Reinforced Polymer (FRP) composites are a class of advanced materials composed of high-strength, continuous fibers embedded within a polymer matrix. The combination results in a lightweight, high-performance material capable of resisting significant tensile forces. FRP composites have gained widespread use in civil engineering, particularly for retrofitting and strengthening of reinforced concrete (RC) structures, due to their favourable mechanical properties, corrosion resistance, and ease of application. Their use reduces the need for heavy machinery, limits labour time, and enables non-intrusive rehabilitation of existing infrastructure[30].

The core principle behind FRP performance lies in the synergy between its constituents. Fibers, such as carbon, glass, basalt, or aramid, provide the tensile capacity, while the polymer matrix distributes stress among fibers, protects them from mechanical and environmental damage, and contributes to overall durability. The matrix also helps maintain the integrity of the composite under varying loads and environmental conditions[30].

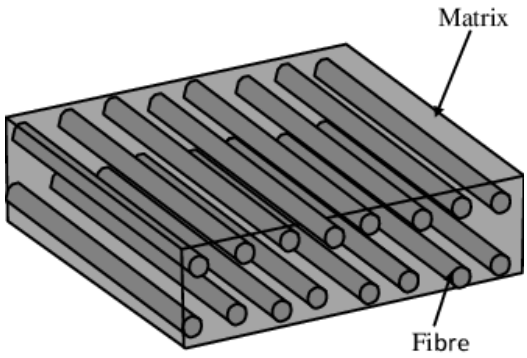

Figure 2.9 Cross-sectional schematic of a unidirectional FRP composite

2.3.2. Types of Fibers and Matrix Materials

The mechanical behavior and durability of FRP systems are heavily influenced by the type of fibers used. Carbon fibers (CFRP) are widely adopted due to their high tensile strength, excellent fatigue resistance, and low weight. They exhibit minimal creep and high modulus of elasticity, making them ideal for structural applications where stiffness is essential. Glass fibers (GFRP) are more affordable and widely available, offering moderate strength and good corrosion resistance, but they tend to have lower stiffness and are more vulnerable to long-term degradation in aggressive environments. Aramid fibers (AFRP) are

known for their impact resistance and fatigue strength, although their performance under UV exposure and alkaline environments is limited. Basalt fibers (BFRP) are emerging as a sustainable alternative, offering better thermal and chemical stability than GFRP with an intermediate cost-performance balance[31], [32].

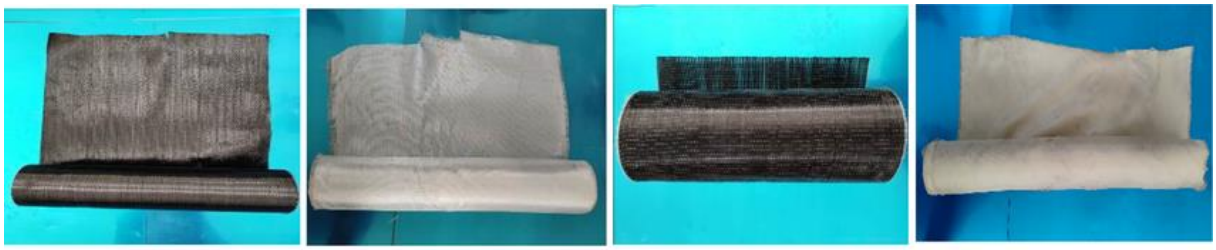

a)CFRP b)GFRP c)BFRP d)AFRP

Figure 2.10 Different Fibers

The matrix material in conventional FRPs is typically a thermosetting resin, such as epoxy, vinyl ester, or polyester. Epoxy resins dominate the field due to their superior bonding ability, mechanical strength, and chemical resistance. However, their use presents challenges under elevated temperatures, exposure to fire, and harsh chemical environments, where degradation of the resin compromises the performance of the entire system. Furthermore, organic polymers are often not compatible with the high pH of concrete, potentially leading to interface degradation over time[33].

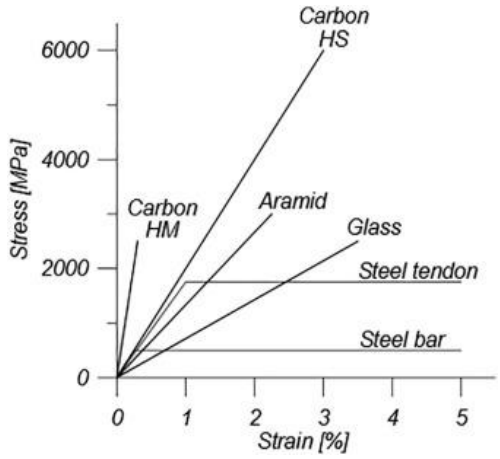

Figure 2.11 Stress-Strain curves of some FRP materials and steel

FRP materials are inherently anisotropic, with their tensile strength and stiffness concentrated along the direction of the fibers. For instance, CFRPs can exhibit tensile strengths exceeding 3000 MPa and elastic moduli up to 230 GPa, surpassing conventional steel reinforcement in tension. However, their performance in compression and transverse directions is significantly lower, making the design process more complex. Unlike ductile materials like steel, FRPs fail in a brittle manner, without yielding or warning, necessitating conservative safety factors and well-defined failure mechanisms in structural applications.

The density of FRP composites is generally low (1.6–2.0 g/cm³), reducing dead load and facilitating transport and installation. Their electrical insulation properties and non-magnetic behavior allow their application in sensitive environments, including hospitals and laboratories. FRPs also exhibit high resistance to corrosion and fatigue, especially in marine and industrial atmospheres, which further supports their use in aging infrastructure[34], [35].

2.3.3. Strengthening Techniques Using FRP

The most common applications of FRP materials in structural strengthening involve two key techniques: Externally Bonded Reinforcement (EBR) and Near-Surface Mounted (NSM) systems. In EBR systems, FRP laminates or sheets are adhered directly to the surface of structural elements using epoxy adhesives. This method is simple, widely practiced, and well-suited for enhancing flexural and shear performance in beams. However, it is susceptible to debonding failures and premature delamination, especially under cyclic or dynamic loading conditions[36].

Alternatively, NSM systems involve embedding FRP rods or strips into pre-cut grooves in the concrete surface, followed by filling the groove with a suitable adhesive. This technique provides enhanced mechanical anchorage, improved bond strength, and better protection against mechanical and environmental damage. NSM systems have shown higher efficiency in certain conditions, particularly for shear strengthening or applications where surface space is limited[37].

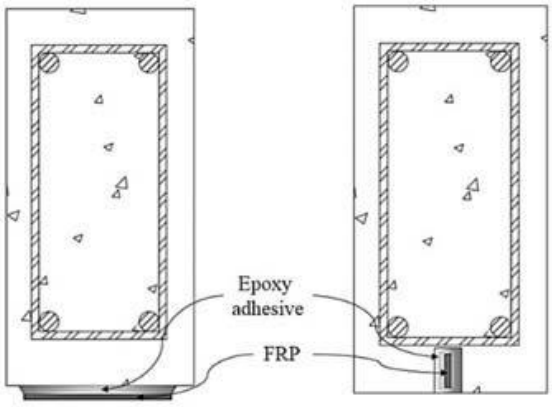

Figure 2.12 NSM and EBR FRP Reinforcement in RC Beam

Both methods are effective in increasing the moment capacity, shear resistance, and ductility of RC beams. They also contribute to improved crack control and deformation compatibility, particularly under service and ultimate load conditions. However, the final performance is significantly influenced by surface preparation, adhesive properties, fiber orientation, and loading conditions[37].

2.4. Fiber Reinforced Cementitious Concrete (FRCC)

2.4.1. Overview and Material Composition

Fiber-Reinforced Cementitious Composites (FRCCs) represent a high-performance category of cement-based materials that integrate discontinuous, short fibers into a cementitious matrix to overcome the brittle nature of conventional concrete. In traditional cementitious materials, cracking initiates and propagates rapidly once the tensile strength of the matrix is exceeded. FRCCs, however, are designed to provide a ductile response under tension, characterized by distributed micro cracking, strain hardening, and enhanced toughness. These unique behaviours make FRCCs particularly suitable for structural strengthening and retrofitting applications, especially in cases where inorganic, durable, and thermally stable materials are required[38].

The effectiveness of FRCCs stems from their careful material formulation. The matrix is typically based on Portland cement, often blended with pozzolanic additives such as silica fume, fly ash, or ground granulated blast furnace slag. These supplementary materials refine the microstructure, enhance matrix-fiber interaction, reduce brittleness, and improve long-term durability. Coarse aggregates are intentionally omitted from FRCC mixes to ensure homogeneity and to facilitate uniform fiber distribution. Instead, fine aggregates—usually silica sand or crushed quartz particles less than 1.2 mm in diameter—are used[39]. Water-to-cementitious material ratios are kept relatively low (often between 0.25 to 0.35) to ensure high strength and low porosity, with superplasticizers used to retain workability. The addition of fibers is the critical feature that transforms the behavior of the composite. A wide variety of fiber types can be used in FRCCs, including polymeric (polypropylene, polyvinyl alcohol), glass, carbon, basalt, and metallic fibers. Among these, steel fibers are of particular interest in structural applications due to their excellent mechanical properties and high stiffness, which allow them to effectively bridge cracks and contribute to post-cracking strength. The aspect ratio (length to diameter) of steel fibers typically ranges from 50 to 100, and the volume fraction commonly varies between 0.5% and 2.5%[38].

Figure 2.13 Typical FRCC with steel fibers

2.4.2. Steel Fibers and Matrix Interaction Mechanisms

The use of steel fibers in FRCCs significantly improves the material's load-carrying capacity, especially in tension and shear-dominated applications. These fibers act as crack arrestors, delaying crack propagation and enabling strain-hardening behavior. Upon the initiation of micro cracks in the matrix, steel fibers bridge the crack openings and carry tensile stress, allowing multiple cracks to develop in a distributed fashion rather than a single dominant crack. This phenomenon enhances not only the tensile capacity but also the energy absorption, post-cracking ductility, and serviceability performance of structural members[40].

Steel fibers come in various geometries, including straight, crimped, twisted, and hooked ends. Hooked-end fibers are particularly effective because they provide mechanical anchorage within the cement matrix, thereby enhancing pull-out resistance and improving the bond performance at the fiber-matrix interface. The performance of the composite is highly dependent on the nature of this interaction, which comprises three main bonding mechanisms: chemical adhesion, frictional resistance, and mechanical interlock[41].

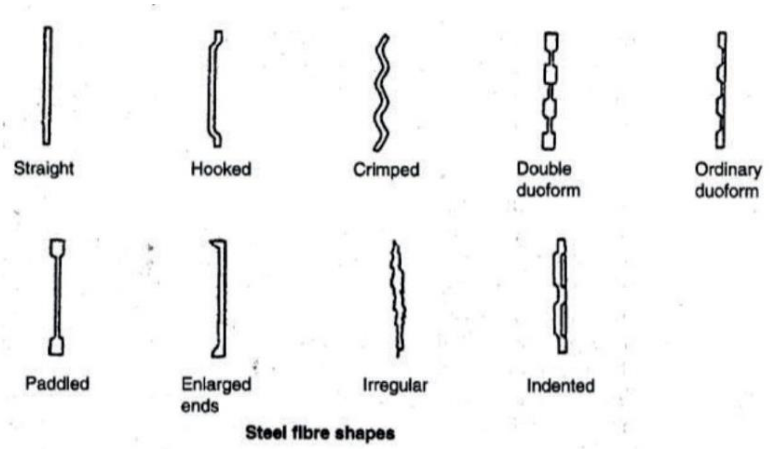

Figure 2.14 Distinct types of steel fibers

Chemical adhesion refers to the bond formed through the hydration products that attach to the fiber surface during curing. Frictional resistance becomes active once the matrix starts to crack and sliding begins at the interface, while mechanical interlock, enhanced by fiber deformation, resists fiber pull-out and contributes to load transfer across cracks. The synergy of these mechanisms determines the fibber's effectiveness in restraining crack widening and controlling crack patterns[42].

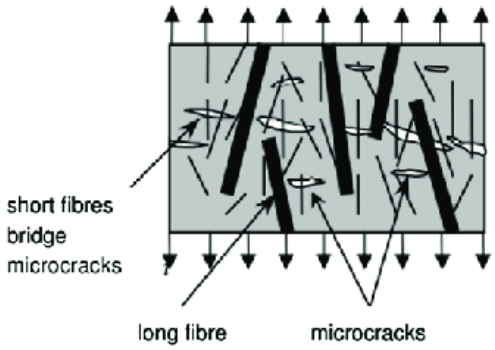

Figure 2.15 Illustration of steel fibers bridging micro cracks

The fiber-matrix interface zone, often referred to as the Interfacial Transition Zone (ITZ), is crucial in defining the performance of FRCCs. Proper dispersion, alignment, and embedment of fibers are essential for maximizing the composite's performance. In practice, achieving uniform fiber distribution and avoiding clumping requires careful control during mixing and casting. Moreover, matrix design must be compatible with the selected fiber type to prevent fiber debonding or premature pull-out under service loads[42].

2.4.3. Tensile Behavior and Mechanical Properties

A defining feature of high-performance FRCCs is their remarkable tensile response. Unlike conventional concrete, which fails in a brittle manner once cracking begins, FRCCs exhibit a strain-hardening behavior under uniaxial tension. Initially, the composite responds elastically. When the matrix cracking strength is reached, a first crack forms. Rather than causing immediate failure, stress is redistributed to surrounding fibers, which continue to carry load, allowing additional micro cracks to form. This continues until the material reaches its peak tensile strength, after which strain localization and softening eventually occur[43].

Table 2.1 Typical Tensile Properties of Steel Fiber-Reinforced FRCCs

Property	Typical Value Range
First Cracking Stress	3 – 5 MPa
Ultimate Tensile Strength	5 – 15 MPa
Tensile Strain Capacity	0.5 – 2.5% (up to 5% in ECCs)
Elastic Modulus	15 – 40 GPa
Fiber Volume Fraction	0.5 – 2.5%
Property	Typical Value Range

This tensile behavior is responsible for the material's high energy absorption and ductility. The crack spacing is typically small, and the crack width is narrow—often below 100 microns—resulting in superior durability by limiting ingress of harmful agents such as chlorides and moisture[44].

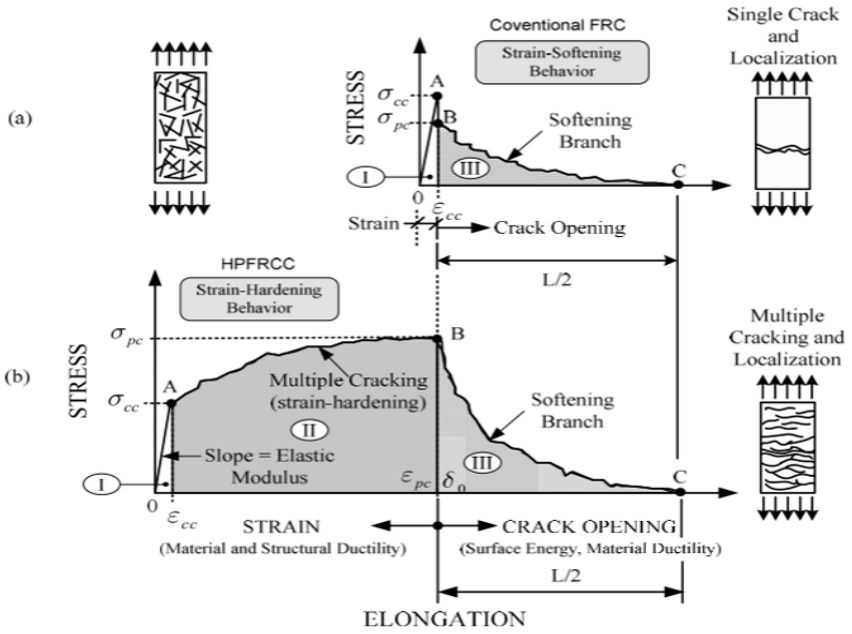

Figure 2.16 Tensile stress-strain behavior of FRCC showing elastic stage, strain hardening, and softening compared to plain concrete.

The exact mechanical performance depends on the fiber characteristics (length, geometry and stiffness), matrix composition, fiber orientation, and curing regime. Steel fibers, with a modulus of elasticity of approximately 200 GPa, are particularly effective in enhancing the elastic stiffness and ultimate strength of the composite, making them an ideal choice for structural retrofitting tasks.

2.4.4. Durability, Fire Resistance, and Environmental Performance

One of the fundamental advantages of FRCCs over organic matrix systems such as epoxy-based fiber-reinforced polymers (FRPs) is their inherent durability and fire resistance. FRCCs are composed entirely of inorganic materials, which are non-combustible, chemically stable, and compatible with concrete substrates. Unlike epoxy resins, which can degrade at temperatures as low as 60–80°C, FRCCs maintain their integrity at elevated temperatures and are suitable for fire-critical infrastructure[2].

Furthermore, the inorganic matrix ensures compatibility in thermal expansion and shrinkage behavior when bonded to RC substrates, minimizing interfacial stress development over time. FRCCs are also immune to ultraviolet radiation, moisture ingress, and chemical attack, making them highly durable in aggressive environments[45].

These properties make FRCCs an ideal solution for strengthening historical or monumental structures where reversibility, material compatibility, and long-term durability are essential. Their use eliminates the long-term aging, debonding, or softening issues associated with synthetic resin systems, enhancing the sustainability profile of the strengthening intervention[46].

2.4.5. Recycling of Tyre cords

The automotive industry's rapid growth has become a major contributor to global waste generation. One significant by-product is used tyres, which are composed of rubber, textile, and steel cords. Due to the non-biodegradable nature of rubber, improper disposal of tyres presents serious ecological hazards. When dumped in landfills, these tyres can release toxic chemicals into the soil and groundwater, posing risks to local ecosystems[47].

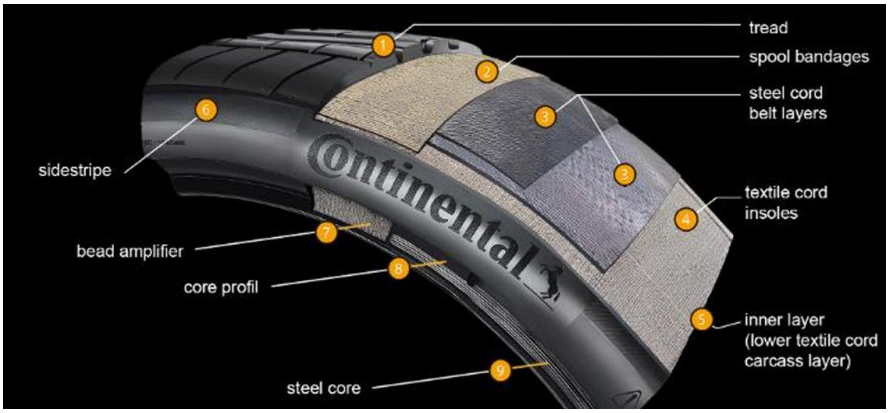

Figure 2.17 Tyre Components

To counter these environmental threats, recycling end-of-life tyres has emerged as a more sustainable and eco-conscious solution. This approach supports the principles of a circular economy by reducing waste, conserving raw materials, saving energy, and cutting greenhouse gas emissions—ultimately leading to less environmental pollution. The recycling process typically includes shredding and separating the tyres into their core components: rubber, textile fibers, and steel cords[48].

Recycled rubber can be repurposed for various applications, while the recovered steel—once considered scrap—is now finding renewed value in the construction sector. Recent research has demonstrated that steel fibers extracted from recycled tyres can effectively replace conventional industrial steel fibers in structural uses, such as enhancing the shear capacity of reinforced concrete beams. These recycled steel fibers have also been shown to improve the toughness and post-cracking behavior of cement-based materials, while reducing their brittleness. Moreover, the use of recycled steel fibers offers a notable economic advantage, as they are significantly more affordable than their industrial counterparts[49].

2.4.6. Application in Strengthening of RC Beams

In structural strengthening applications, FRCCs can be used as overlays, jacketing systems, or sprayed layers on RC elements to enhance flexural and shear capacities. When applied to the tension zone of RC beams, steel fiber-reinforced composites provide additional tensile resistance after concrete cracking, thereby increasing ultimate load capacity, reducing deflection, and enhancing energy dissipation[50].

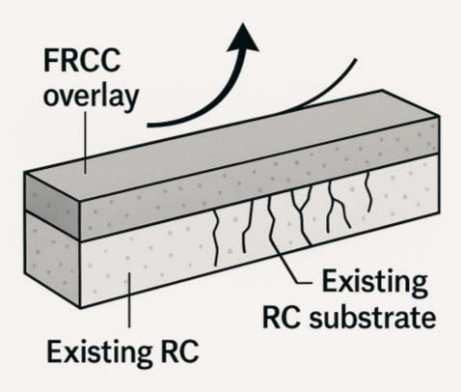

Figure 2.18 FRCC Configuration as Strengthening

The inclusion of fibers also leads to better crack control and improved serviceability by limiting crack widths under service loads. For seismic applications, the strain-hardening and energy-absorbing behavior of FRCCs improves ductility and resistance to repeated loading. Their use has also been explored in hybrid systems combining steel rebars and textile reinforcements for increased performance[51].

Given these advantages, FRCCs—especially those reinforced with steel fibers—are now considered a strategic material for future infrastructure maintenance, retrofitting, and resilience improvement projects.

2.5. Previous Studies

Mu et al. investigated the flexural performance of RC beams retrofitted with sprayed Fiber-Reinforced Cementitious Composites (FRCC), focusing on both intact and pre-cracked conditions. The study used 20 mm and 30 mm thick sprayed overlays applied to RC beams and monitored crack behavior using Digital Image Correlation during flexural testing. Results showed that a 30 mm FRCC layer restored over 85% of original capacity in damaged beams, significantly increased load-bearing performance, and improved crack control and ductility, demonstrating the effectiveness of FRCC for structural rehabilitation under flexural demands[50].

Zhang et al. explored the seismic retrofitting of precast RC beam–column joints using Engineered Cementitious Composites (ECC) reinforced with Shape Memory Alloys (SMA). Full-scale joint specimens were subjected to reverse cyclic loading, and their responses were compared against conventional and

ECC-only counterparts. The SMA–ECC hybrid joints exhibited superior energy dissipation, reduced residual drifts, and improved ductility, highlighting the potential of combining smart materials with FRCC to enhance seismic resilience and self-centering capabilities[52].

Atmajayanti et al. examined the flexural strengthening of RC T-beams using bonded fiber-core steel-wire ropes (FC-SWR). In four-point bending tests, beams reinforced this way showed increased crack initiation load, yield strength, ultimate load, stiffness, and energy absorption. An analytical model based on Modified Compression Field Theory accurately predicted performance. FC-SWR strengthening enhanced flexural response by up to 50%, with improved crack control, although higher rope stiffness reduced ductility[53].

Khattak et al. conducted experimental and numerical studies on continuous RC beams strengthened in sagging or hogging regions using Fabric-Reinforced Cementitious Matrix (FRCM) systems. Two-span beams with two layers of carbon- or PBO-based FRCM in sagging zones saw 17–28 % increases in load capacity, while hogging strengthening achieved 9–17 % gains. Numerical models (ATENA) accurately predicted capacities (within 12%), though deflection was slightly underestimated, emphasizing the role of interface bond–slip behavior[54].

Tian et al. explored the flexural synergistic effect of ECC overlays on damaged RC beams under repeated loading. They retrofitted pre-cracked beams with ECC strips and subjected them to cyclic loading tests, closely monitoring load–deflection responses and crack patterns. The retrofit significantly improved ultimate load capacity (~30%), reduced crack widths, and enhanced strain-hardening behavior, demonstrating ECC's effective rehabilitation potential for structurally compromised beams[55].

Chidambaram & Agarwal conducted an experimental study on RC beams incorporating high-performance FRCC or hybrid FRCC at hinge regions. Seven types of FRCC, including hybrid fibers, were embedded in 26 beams tested under monotonic flexure. They found superior post-yield stiffness, improved ductility, and reduced damage ratios compared to conventional RC, confirming FRCC's capability in enhancing flexural resilience[56].

Wasef et al. evaluated RC beams strengthened with textile-reinforced strain-hardening geopolymer composites (TR-SHGC) under static flexure. Ten beams were tested—including EB and NSEEB techniques—with varying textiles and composite types. Results showed NSEEB-SHGC overlays enhanced ultimate load and ductility by ~67%, and a proposed flexural capacity model calibrated accurately with observed behavior[57].

Baraghith et al. investigated the shear and flexural behavior of RC dapped-end beams strengthened with precast strain-hardening cementitious composite (P-SHCC) plates. Under static loading, strengthened

specimens showed 20–35 % improvement in shear capacity and finer crack distributions in flexure, attributed to P-SHCC's strain-hardening and mechanical interlock with the substrate[58].

Mandor & El Refai studied continuous RC beams strengthened in both hogging and sagging regions using FRCM. Experimental and analytical results showed sagging strengthening improved mid-span flexural capacity by ~25 %, while hogging region strengthened beam-column connections improved hogging moment resistance by ~18 %. Bond-slip behavior and anchorage were identified as critical for performance[59].

Liu et al. examined the flexural behavior of composite beams created using 3D-printed Engineered Cementitious Composite (ECC) layers over recycled fine aggregate concrete (RFAC) cores. Beams with varying ECC overlay thicknesses (15 mm, 30 mm, and 45 mm) were tested under flexure to evaluate structural performance. Results showed that beams with 30 mm and 45 mm ECC layers achieved flexural capacities comparable to RC beams with a steel reinforcement ratio of 0.2%, along with significant ductility improvement. The study emphasized the importance of interfacial bonding between the ECC and RFAC layers in maintaining composite action[60].

Bai et al. investigated the flexural performance of composite beams using 3D-printed U-shaped ECC formworks filled with recycled concrete. The study assessed different ECC formwork geometries and thicknesses under monotonic flexural loading to determine their impact on load capacity and ductility. Beams with 20% ECC formwork height and 30 mm sidewall thickness demonstrated similar performance to traditional RC beams (with 0.3–0.4% reinforcement ratio), while also showing increased peak displacements and improved energy absorption. However, interfacial bond strength between the ECC shell and concrete core was a key limiting factor in structural efficiency[61].

3. EXPERIMENTAL TESTING

The experimental tests conducted in this thesis are a part of series of tests which has been done and continued over the recent years. Even though some of these tests are performed before this study, some of the results are used for validation and calibration of FEA. All the experimental tests of this campaign are illustrated in table3.1. The first test in the series is the flexural test on an unstrengthened RC beam, which serves as the reference specimen to evaluate the baseline performance. It provides essential data on cracking load, ultimate load, and ductility before any strengthening intervention. The second and third tests focus on beams strengthened with EBR and NSM CFRP systems, respectively. The tests were performed to compare their effectiveness in improving load capacity and controlling crack propagation.
The fourth and fifth tests involve RC beams strengthened using a FRCC applied in a U-jacketing configuration with two different steel fiber ratios, 1.1% and 2.0%. These tests aimed to assess how increasing the steel fiber content affects the flexural response, post-cracking behavior, and energy absorption capacity of the beams. The sixth and seventh tests, conducted within the scope of this thesis, introduce a hybrid strengthening approach combining steel fibers and PE fibers. In Test 6, a U-jacketing configuration with 1.1% steel fibers and 1.0% PE fibers was applied, while in Test 7, the same hybrid composite was used as a bottom reinforcement layer.

Table 3.1 *Experimental test Campaign*

Number	Experimental Test	Status	Correlation with current study
1	RC Beam (Flexural Test)	Completed Before	Used
2	RC Beam Strengthened with CFRP EBR	Completed Before	Used
3	RC Beam Strengthened with CFRP NSM	Completed Before	Used
4	RC Beam Strengthened with FRCC U Jacketing (1.1% Steel Fiber ratio)	Completed Before	Used
5	RC Beam Strengthened with FRCC U Jacketing (2% Steel Fiber ratio)	Completed Before	Used
6	RC Beam Strengthened with FRCC U Jacketing (1.1% Steel Fiber + 1% PE Fiber)	Completed In This Thesis	Used
7	RC Beam Strengthened with FRCC Bottom reinforcement (1.1% Steel Fiber + 1% PE Fiber)	Completed In This Thesis	Used

3.1. Material Characterisation

The starting point of experimental test is the material characterisation which is done in the form of three point bending. The results obtained from this test is used to understand the behavior of material itself in a proper way. Afterwards, the properties taken from this part is taken to the beam testing for proper analysis of the beams.

3.1.1. Geometry and Material

The specimens used in this test are three rectangular cubes with 40 × 40 mm cross section and 160mm length. Due to uncertainty in the test three similar specimens have to be tested and the average of results can be considered as the final value. The dimensions of the specimens are shown in figure3.1.

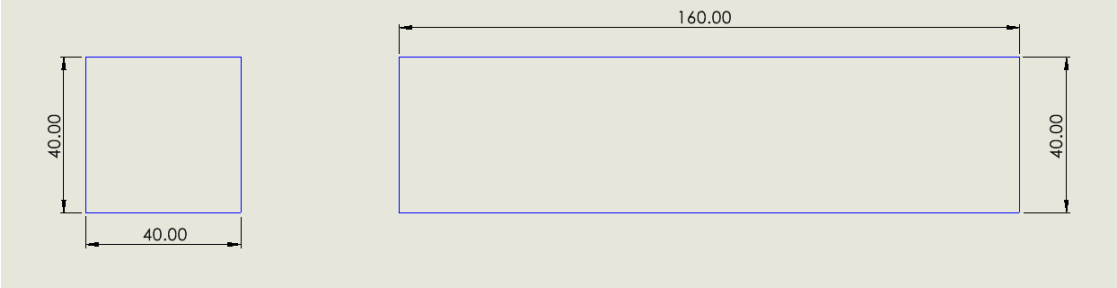

Figure 3.1 Specimen Dimensions

The material used in this test is FRCC with 2.1% fiber ratio (1.1% steel fiber + 1% PE fiber). The composite material used is consist of recycled steel fibers from tyre cords, PE fibers and an ultra-high-performance cementitious mortar. The matrix in this application is "MAPEI PLANITOP HPC", an ultra-high performance, Shrinkage-compensated, free-flowing, and self compacting cementitious mortar. Incorporating recycled steel fibers aligns with the principles of a circular economy, helping to lower greenhouse gas emissions and minimize environmental impact while fostering sustainable structural solutions. The configuration of the steel fibers are shown in figure 3.2.

a) Fiber Bundle

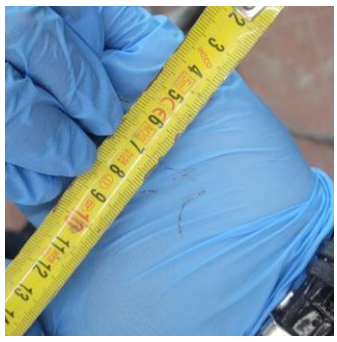

b) Fiber sizing

Figure 3.2 Steel fibers

As it can be seen in the figure 3.2 b, the steel fibers configuration are hooked end which enhances the quality of bond between the mortar and the fibers. Moreover, the properties of steel fibers are shown in table 3.2.

Table 3.2 Mechanical properties of steel fibers

Tensile Strength (Mpa)	2000
Modul of Elasticity (Mpa)	200000

Furthermore, Polyethylene (PE) fibers are lightweight synthetic fibers with high tensile strength and excellent resistance to moisture and chemicals. When incorporated into cementitious composites, they improve crack control, ductility, and overall durability, making them suitable for long-term structural applications.

a) Fiber sizing

b) Fiber Bundle

Figure 3.3 PE fibers

After all the raw materials are ready, the mortar and water are added to the mixer and will be mixed for 8 minutes. After that, the fibers are added to the mixure over time and 5 to 10 minutes is given to provide an even texture for the FRCC. It should be noted that due to the water absorbing nature of the PE fibers, the amount of required water for the mortar is more than the standard value. The procedure and the final outcome of FRCC is shown in figure 3.4.

a) Mixing mortar with fibers

b) FRCC Texture

Figure 3.4 FRCC 2.1%

Following this, FRCC is poured into the prepared molds and in order to remove the excess air tarpped inside, manual methods plus a vibrator is used to provide a good quality for the specimen. Finally, the specimens require 21 days to be cured properly, however, due to some urgencies, the test was done 12 days after the casting. As a result, it resulted in lower mechanical properties for FRCC and reduction in poperties should be considered.

a) Before using vibrator b) After using vibrator c) Final Specimens

Figure 3.5 FRCC 2.1% Casting

3.1.2. Test set up

The three-point bending test is a widely used experimental method to determine the flexural properties of materials such as composites, mortars, and concrete. In this test, the specimen is supported at two points, creating a simply supported beam configuration, while a concentrated load is applied at the mid-span through a loading nose. This setup induces both bending and shear stresses, with the maximum bending moment occurring at the mid-span.

The three-point bending machine consists of a rigid loading frame, two adjustable supports to hold the specimen, and a loading actuator or crosshead that applies the force at a controlled rate. A calibrated load cell measures the applied load, while deflection at the mid-span is recorded using a displacement transducer or the machine's built-in displacement sensors. Data acquisition software is typically used to capture the load–deflection response throughout the test.

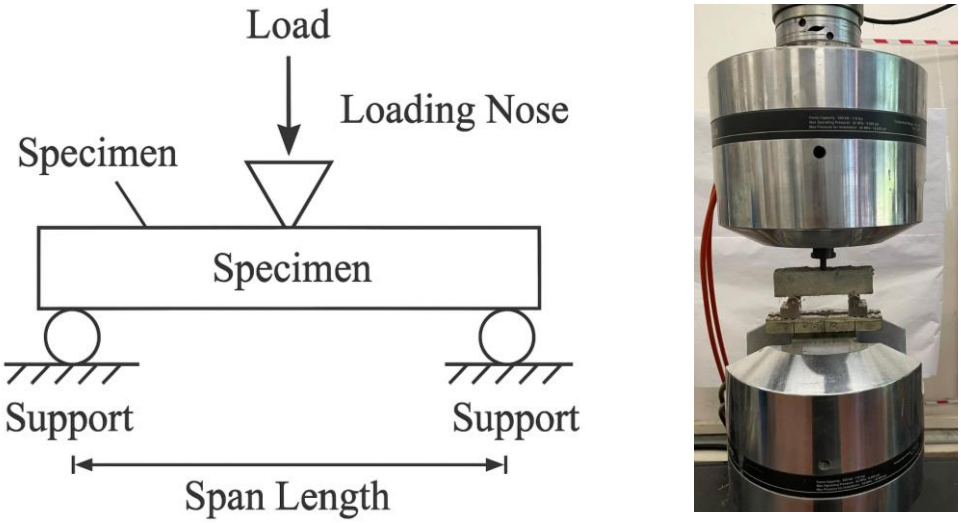

Figure 3.6 Three Point bending Machine

This test allows for the determination of important parameters such as the flexural strength, which corresponds to the maximum load sustained before failure, and the modulus of elasticity, calculated from the slope of the initial linear portion of the load–deflection curve. Additionally, it provides valuable information on the material's cracking behavior, ductility, and failure mode, such as brittle fracture, fiber pull-out, or delamination. The simplicity of the setup and the ability to simulate real bending conditions make the three-point bending test an effective choice for characterizing cementitious composites and fiber-reinforced materials.

The test was done for three specimens up to failure and after the test was done, all specimens were cut into half from the major crack position and then were used for the compression test (with the same machine only different head) in order to obtain the compressive strength of FRCC 2.1%. The Tested Specimens that the ones prepared for compression test are shown in figure 3.7.

a) Specimen under test b) All tested Specimens c) Preparation for compression test

Figure 3.7 Tested Specimens

The six prepared specimens are then put into the machine again for the compression test. The figure 3.8 demonstrates the set up for the test.

a) Testing Machine b) Tested Specimens

Figure 3.8 Compression test

3.1.3. Results

The three-point bending tests conducted on the specimens exhibited a typical load–displacement response characteristic of fiber-reinforced cementitious composites. In the initial stage, all three samples showed a linear elastic behavior up to a displacement of approximately 1.5 mm, indicating a similar flexural stiffness and confirming the consistency of material properties and specimen preparation.

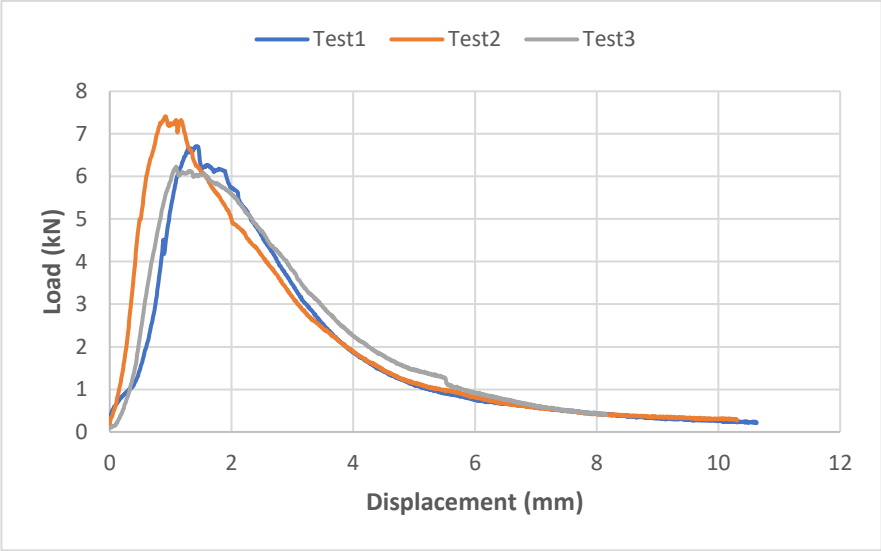

Figure 3.9 Load vs Displacement curve of three Point Bending

Beyond the elastic range, each specimen reached a distinct peak load, corresponding to the flexural strength of the material. Among the three tests, Test 2 reached the highest peak load of approximately 7.5 kN, followed by Test 3 at about 6.8 kN, while Test 1 exhibited the lowest peak load of around 6.3 kN. This variation, although present, remains within an acceptable range for experimental composites and

may be attributed to minor differences in material distribution or local defects. The displacement at peak load was around 1.5–2.0 mm, suggesting a semi-brittle failure mode typical of inorganic composite materials.

After reaching the peak, all specimens demonstrated a gradual softening behavior rather than a sudden drop in load, highlighting the presence of residual load-carrying capacity even after the initiation of flexural cracks. This post-peak behavior can be attributed to the fiber bridging effect, which delayed complete failure and allowed the material to sustain additional deformation. The residual strength converged across all tests, with the load gradually decreasing to around 1 kN at 6 mm displacement and approaching zero near 10 mm.

The overall shape of the curves reflects the energy absorption capability and ductility improvement imparted by the fibers. Test 2, with the highest peak load, also exhibited a slightly larger area under the curve, indicating superior toughness compared to the other two specimens. The absence of abrupt brittle failure and the presence of a long softening tail confirm the beneficial role of fiber reinforcement in improving post-cracking behavior, enhancing both ductility and crack resistance.

The compression test results presented in Table 3.3 show the residual compressive capacity of the specimens after they were previously tested in three-point bending. The average maximum compressive force recorded was 110.6 kN, corresponding to an average compressive strength of 71.5 MPa. Despite prior flexural loading, the specimens retained a significant portion of their compressive strength, indicating good damage tolerance and post-bending structural integrity.

Table 3.3 Compression test results

Specimen	Max Force (kN)	Max compressive Strength (Mpa)
1	120	75
2	93	58
3	111	70
4	108	67.5
5	119	74
6	113	70.6
Average	110.6	71.5

Among the six specimens, Specimen 2 exhibited the lowest compressive strength of 58 MPa (93 kN), which is noticeably below the average. This reduction is likely due to more severe cracking or internal micro damage accumulated during its bending test. In contrast, Specimens 1 and 5 showed the highest

residual compressive strength values, reaching 75 MPa and 74 MPa respectively, suggesting that they experienced less extensive damage during flexural loading.

The variation between specimens remains within a reasonable range, except for Specimen 2, which is considered an outlier. Overall, the results demonstrate that prior bending-induced damage did not completely compromise the compressive performance of the material. The retention of over 90% of the original compressive strength for most specimens highlights the robustness of the FRCC and its ability to sustain multiple loading types without catastrophic degradation.

3.2. Beam Testing

Following the material characterization of FRCC 2.1% material, the scaled beams with U-jacketing and bottom reinforced with FRCC is the next test case. The test is conducted with four point bending machine and 2 beams are tested in total. Moreover, the DIC results are shown in the last section.

3.2.1. Geometry and Materials

The beams length are 1500mm and cross section of 180 × 100 mm. the beams are consist of 13Ø8 stirrups and 2Ø8 for top and bottom steel longitudinal reinforcement. Moreover, the concrete cover is 20mm. All the details are shown in figure3.10.

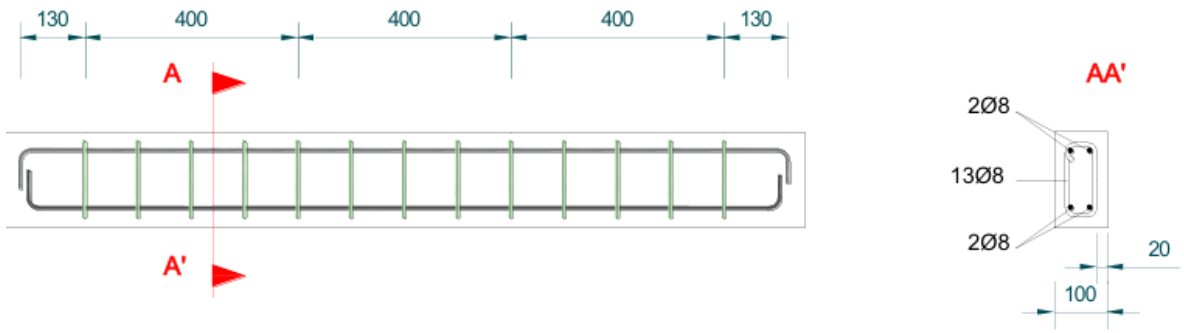

Figure 3.10 Geometry of the Beam

The concrete grade chosen for the beams is C25/30 and all the properties required for the concrete are shown in table3.4. Furthermore, the FRCC 2.1% for strengthening is characterized in section3 and same material is used for the beams.

Table 3.4 Concrete C25/30 mechanical properties

ρ (kg/m³)	f_{ck} (Mpa)	f_{cm} (Mpa)	E_c (Gpa)
2450	25	33	34

The reinforcement steel used is B450C. The density (ρ), the characteristic yield strength (f_{yk}), the characteristics ultimate strength (f_{uk}), the Characteristic yield strain (ε_{yk}), the Characteristic ultimate strain (ε_{uk}) and the modulus of elasticity (E_s) of this conventional reinforcing steel according to [62] are summarized in Table 3-5.

Table 3.5 Steel B450C mechanical properties

ρ (kg/m³)	F_{yk} (Mpa)	F_{uk} (Mpa)	E_s (Gpa)	ε_{yk} (%)
7850	450	650	210	0.28

The RC beams were already cast and cured under standard conditions for 28 days before the strengthening process. To prepare them for FRCC application, the existing concrete cover in the designated strengthening zones was carefully removed using mechanical means. This process exposed the aggregate surface and, in some areas, partially revealed the longitudinal reinforcement. Removing the cover ensured better mechanical interlocking and composite action between the original concrete substrate and the newly applied FRCC layer. By replacing the original cover, the FRCC could bond directly to the core concrete and reinforcement, minimizing any weak interface that might reduce the strengthening efficiency.

Figure 3.11 Concrete Cover removal

Following the cover removal, the framework in which the FRCC is going to be casted is prepared. Based on the removed thickness of the concrete and desired outcome thickness of the FRCC, the wooden framework is around the beams.

Figure 3.12 FRCC Framework

For the first beam, an FRCC layer was applied only to the tension face (bottom surface), acting as additional tensile reinforcement and improving the flexural capacity in the critical tension zone. The second beam was strengthened using a U-jacketing configuration, where the FRCC layer covered not only the bottom surface but also extended up both vertical sides. In both cases, the FRCC mix consisted of cementitious matrix with 1.1% steel fibers and 1% polyethylene fibers by volume, cast to a uniform thickness of 50mm for bottom reinforcement and 30mm for bottom side of the U-jacketing and 20mm for the sides. Beam are cured unitl 12 days before testing. The preparation process of FRCC is not mentioned in this section because it was explained in secion 3.1. The visual process of FRCC casting into the beams are shown in figure 3.13. Also, PE fibers increased the viscousity of the FRCC mixure and as a result the casting process became more difficult. For solving this issue, a strong vibrator is used to eliminate voids inside the FRCC and increase the casting quality.

Figure 3.13 Visual process of FRCC casting

After the casting and curing process was completed, the middle region of each beam—corresponding to the constant moment zone in the four-point bending test—was prepared for digital image correlation (DIC) measurements. This optical technique requires a high-contrast, random speckle pattern on the surface to accurately track deformations during loading.

Figure 3.14 DIC Zone identification and clearance

To create the speckle pattern, the surface of the beam was first cleaned to remove any dust or loose particles. Then, a random distribution of small black dots was carefully sprayed over the surface, forming a unique, non-repetitive spe+ckle pattern. This pattern ensures that the DIC system can recognize and track surface displacements and strain fields with high precision.

Figure 3.15 Speckle pattern

The speckle-patterned area was aligned with the field of view of the DIC cameras during the test. High-resolution images were captured continuously throughout the loading process, allowing the system to calculate full-field strain and displacement maps in the constant moment region. This approach provided detailed insights into the crack initiation, propagation, and deformation behavior of the strengthened beams.

3.2.2. Test set up

The four-point bending test is a standard experimental method used to evaluate the flexural behavior of structural elements such as reinforced concrete beams. In this setup, the beam is simply supported at two ends while two equal loads are applied symmetrically at one-third of the span length. This loading configuration creates a constant moment region between the two loading points, minimizing shear effects

in the central zone. It allows for a clearer observation of flexural cracking, stiffness degradation, ductility, and ultimate load capacity.

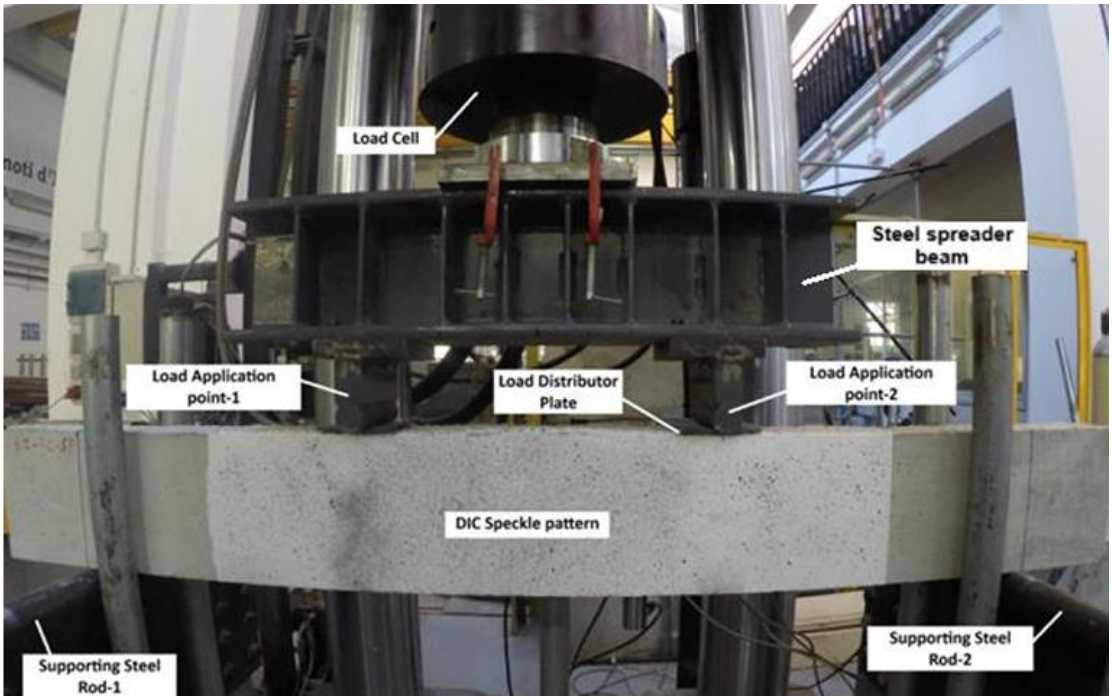

Figure 3.16 Four point bending test machine configuration

The test was conducted using a universal machine 'ITALSIGMA' with a load capacity of 3000 kN. Since the estimated failure loads for each specimen were very small compared to the full loading capacity of the machine, load cells were used for more accurate load measurements. Two steel roller supports were used to simulate simple supports, while the loading system consisted of a rigid spreader beam that divided the applied load equally between the two loading points. The clear span of the beam was 1500mm, with the two loading points positioned 400mm from the support, creating a constant moment region in the middle of the beam.

During testing, the load was applied under displacement control at a rate of 2 mm/min to capture the complete load–deflection response, including post-peak behavior. Mid-span deflection was recorded using a linear variable displacement transducer (LVDT), while additional LVDTs were placed at the loading points to monitor local deformations. For full-field surface strain analysis, a digital image correlation (DIC) system was employed in the constant moment zone. The applied load, deflection, and strain data were continuously collected by a data acquisition system throughout the test.

a) DIC camera set up

b) LVDT positions

Figure 3.17 Four point bending test set up

Following that the beams are tested up to failure and results obtained from the test machine and DIC are discussed in the upcoming sections.

a) Bottom reinforcement

b) U-Jacketing

Figure 3.18 Failure scene of tests

3.2.3. Results

The load–displacement responses of the two strengthened beams—one with a 50 mm bottom FRCC layer and the other with a 30 mm U-jacketing layer—show similar overall trends, with an initial linear elastic stage, a peak load plateau, and a gradual softening followed by large post-peak deformation capacity.

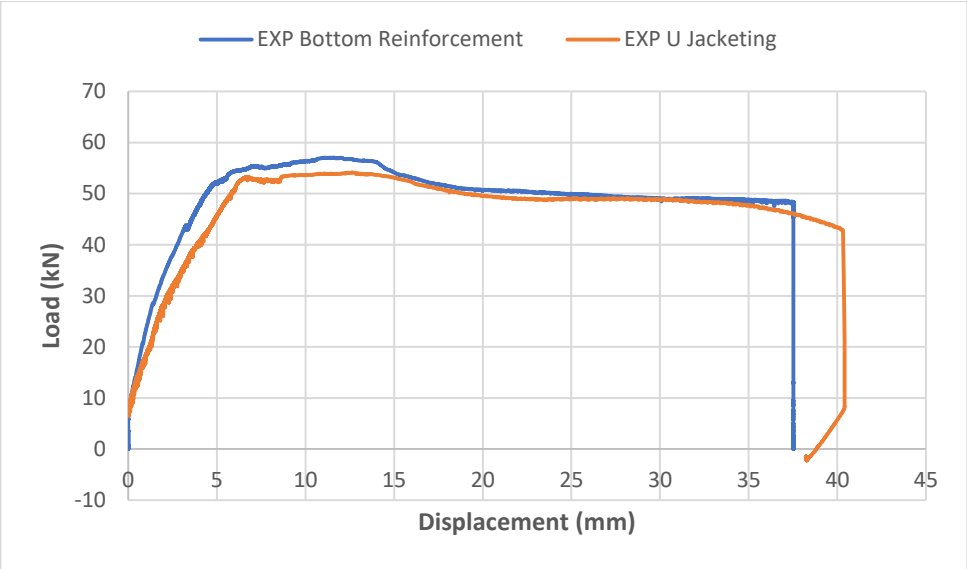

Figure 3.19 Force vs Displacement RC beams strengthened with 2.1%FRCC

In the initial elastic region (0–5 mm displacement), both beams exhibited comparable stiffness, indicating that despite the difference in FRCC thickness, the two strengthening configurations provided similar initial flexural rigidity before cracking. This suggests that in the pre-cracking phase, the contribution of the FRCC layer's thickness is less significant compared to the overall section stiffness dominated by the original RC section.

After cracking, bottom reinforcement reached a slightly higher peak load of approximately 58 kN, while U-jacketing peaked near 55 kN. This represents an almost 7% higher peak strength for the bottom reinforcement. The increased thickness directly enhances the tensile capacity in the most critical zone, explaining the marginally higher flexural strength.

These results suggest that although the thickness of U-jacketing is much smaller than the bottom reinforcement, the peak capacities are close to enough to conclude that the U-jacketing provides better overall performance in terms of ductility and peak capacity.

3.3. Digital Image Correlation Results

Digital Image Correlation (DIC) is a non-contact optical measurement technique used to obtain full-field surface displacement and strain during mechanical testing. Unlike conventional sensors such as strain gauges or LVDTs, which provide data at discrete points, DIC captures the deformation of the entire region of interest (ROI), enabling a more detailed understanding of the structural response. It has become an essential tool in experimental mechanics for validating numerical models, visualizing crack propagation, and quantifying local strain concentrations.

3.3.1. Principle of Operation

The working principle of DIC is based on optical tracking of a random speckle pattern applied to the specimen's surface. Before testing, the ROI is coated with a uniform white base layer, followed by randomly sprayed black speckles to create a unique high-contrast pattern. This pattern allows the software to recognize and track small image subsets (known as facets) during deformation.

As shown in Figure 3.20, the DIC system acquires a reference image of the undeformed specimen at the beginning of the test. During loading, sequential images are captured at defined time intervals. The DIC algorithm then compares each small facet in the reference image with its corresponding facet in the deformed images using a cross-correlation function. By identifying the shift of each facet, the software computes local displacements in the X and Y directions. Numerical differentiation of these displacement fields yields the strain maps, such as normal strain, shear strain, and principal strain.

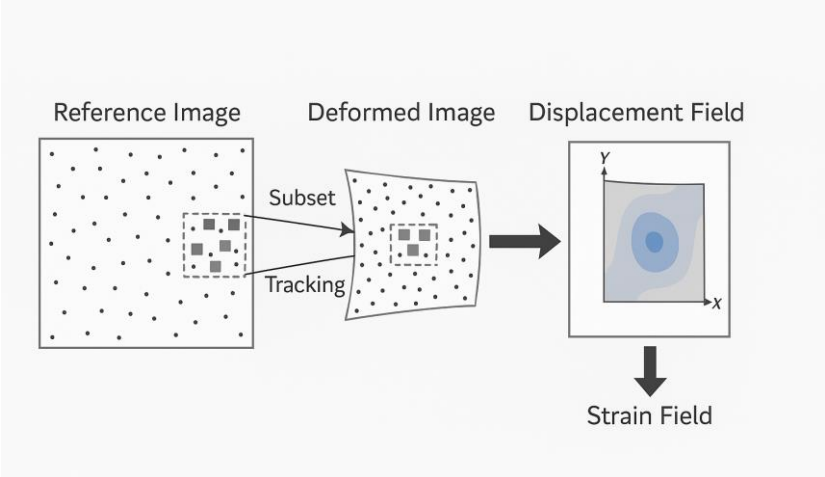

Figure 3.20 Schematic of DIC working principle

Depending on the application, DIC can be implemented in two configurations:

- 2D DIC, using a single camera, is suitable for planar specimens undergoing in-plane deformation with minimal out-of-plane motion.
- 3D DIC, using a stereo camera setup, enables full three-dimensional displacement and strain measurement, including out-of-plane movements.

3.3.2. Test Setup and Implementation

For the four-point bending tests, the middle region of the beam—coinciding with the constant moment zone—was selected as the ROI. This area was prepared with a random black speckle pattern to achieve

contrast for image tracking. A high-resolution digital camera was positioned perpendicular to the beam surface, ensuring the entire ROI remained in the field of view.

As illustrated in Figure 3.17, the camera was mounted on a stable tripod outside the test rig, and the lighting conditions were controlled to eliminate glare and shadows that could interfere with image quality. During loading, the camera continuously recorded images at a frequency of 1 frame per 5 seconds, capturing the gradual development of cracks and surface deformation.

The recorded images were later processed using ZEISS software, where parameters such as facet size, step size, and correlation algorithm were carefully selected to balance accuracy and computational efficiency. The output included full-field displacement maps, strain contours, and crack evolution visualization, providing valuable insight into the flexural behavior of the strengthened beams.

3.3.3. Results

In this study, the 2D DIC was conducted using a single camera in the middle section of the beam. At the beginning, the strain contour at the starting point of cracking in tension part was considered in order to obtain the max tensile capacity of the FRCC 2.1% material. Based on hook's law, the maximum stress before the cracking begins, equal to corresponding strain multiplied to the young's modulus. The young's modulus of the material is assumed same as the FRCC 2% material which is 16.4 GPa. As shown in figure 3.21, the max strain of the beam with bottom reinforcement is 0.037% which is happening in point4. As a result, the maximum tensile capacity of the FRCC 2.1% is calculated as 6.068 MPa. Although, there might be some inaccuracies (due to the fact that the bottom part is not pure tension) in this method for obtaining the maximum tensile strength, it is a good initial value for start of the investigation.

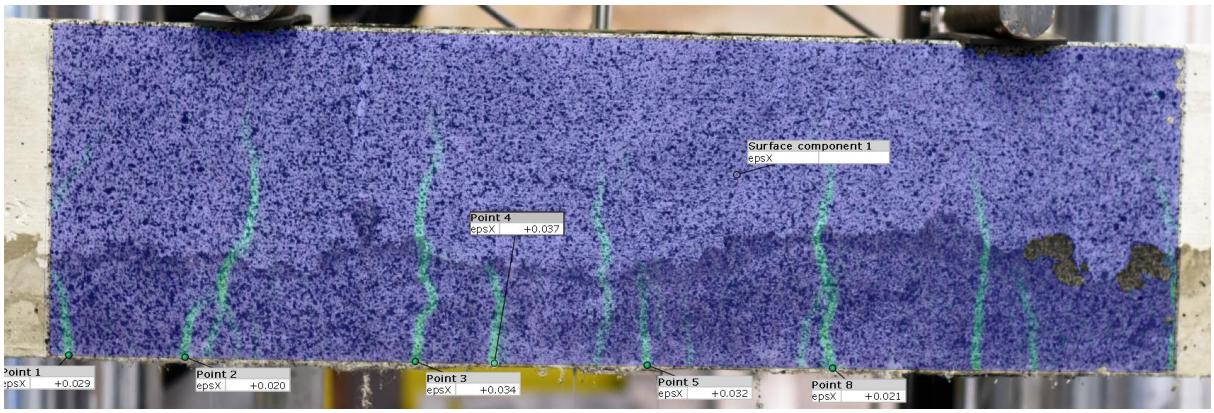

Figure 3.21 Strain contour of the bottom reinforced beam

The same analysis was conducted for the U-jacketing and the result is demonstrated in figure 3.22. The maximum strain obtained is 0.038% which result in 6.232 MPa maximum tensile strength. As the both

DIC results illustrate, values for tensile strength are close to each other and it confirms that the value is reliable.

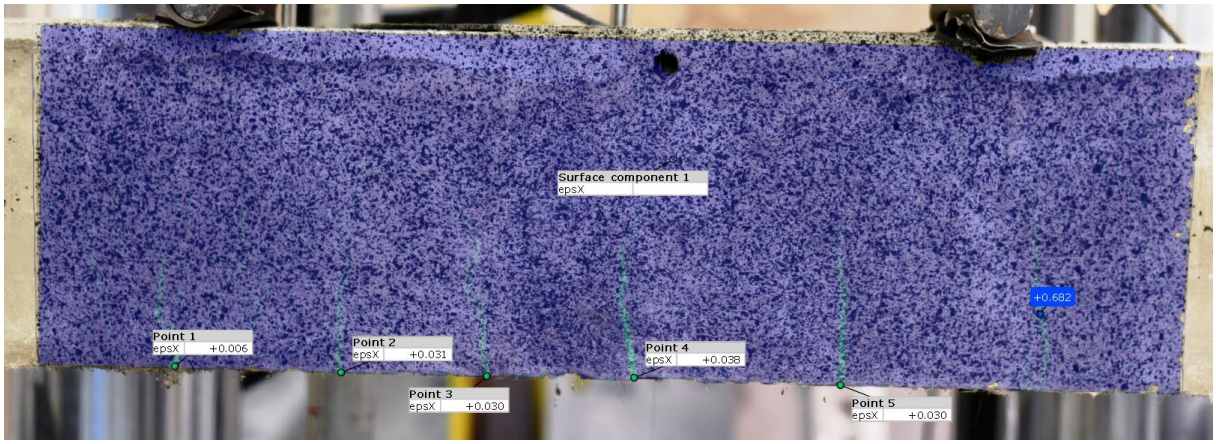

Figure 3.22 Strain contour of the U-Jacketing

Following that, the principal strain distribution of both beams at failure are shown in figure 3.23 and 3.24. For the bottom reinforced beam , the strain distribution shows a series of well defined vertical flexural cracks concentrated primarily within the constant moment region. Moreover, The strain intensity reaches its maximum near the mid-span, where the bending moment is highest.

In contrast, the U-jacketed beam exhibits a denser network of finer cracks, with lower strain concentration at each individual crack. The red strain bands are less pronounced, and the cracks appear more evenly distributed along the constant moment region. This behavior reflects the confinement effect provided by the U-jacketing, which helps redistribute tensile stresses more uniformly and delays the formation of a single critical crack.

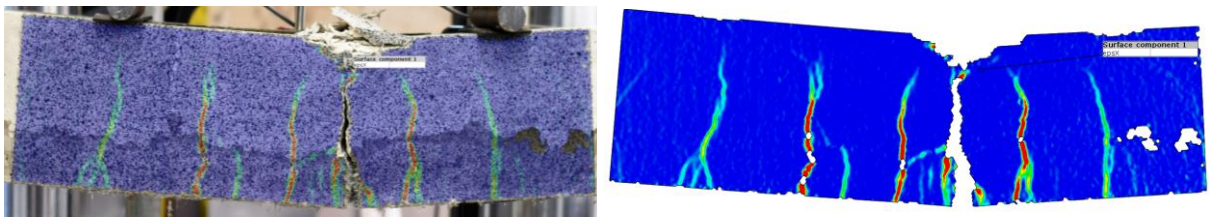

Figure 3.23 Principal strain distribution for bottom reinforced beam at failure

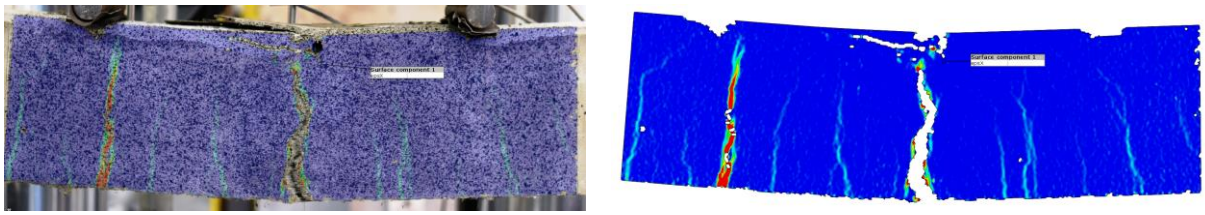

Figure 3.24 Principal strain distribution for U-jacketing at failure

Comparison:

- The bottom reinforcement results in fewer but wider cracks, indicating higher localized strains and more brittle crack propagation.
- The U-jacketing leads to multiple, finer cracks with more uniform strain distribution, demonstrating better control of crack growth and improved ductility.
- Despite being thinner (30 mm vs. 50 mm), the U-jacketing is more effective in controlling crack propagation and maintaining structural integrity in the post-peak phase due to its confinement effect.

THIS PAGE WAS INTENTIONALLY LEFT BLANK

4. NUMERICAL MODELLING

To complement the experimental investigations and gain deeper insight into the structural behavior of the strengthened beams, a comprehensive finite element model (FEM) was developed using ABAQUS. This numerical simulation aims to replicate the nonlinear flexural response of RC beams retrofitted with both bottom reinforcement and U-jacketing techniques under four-point bending and perform a parametric analysis afterwards.

The FEM approach allows for a detailed assessment of stress distribution, crack formation, and damage evolution, offering a powerful tool to predict behavior beyond what can be directly measured in experiments. ABAQUS, with its robust capabilities for nonlinear material modelling and contact interactions, provides an ideal platform for simulating complex behaviors such as cracking, crushing, debonding, and strain localization in reinforced concrete structures.

The model incorporates realistic representations of concrete, steel reinforcement, and the FRCC, along with proper boundary conditions, interaction definitions, and material constitutive laws. Calibration was performed using experimental data to validate the accuracy and reliability of the simulation results, ensuring the model can serve as an effective extension of the physical testing.

4.1. Bare Beam (Flexural Behaviour)

As an initial step in the numerical investigation, a finite element model of a RC beam without any FRCC strengthening was developed using ABAQUS to serve as a baseline for validation and calibration. This model replicates the geometry, reinforcement detailing, boundary conditions, and loading scheme of the corresponding experimental beam tested under four-point bending. The primary objective of this initial simulation was to verify the accuracy of the material models, mesh sensitivity, and nonlinear behavior implementation—particularly the concrete cracking and steel yielding mechanisms. The results obtained from this unstrengthened RC beam model were compared with experimental force vs displacement curves to ensure that the simulation framework is reliable before proceeding to the modeling of strengthened specimens.

4.1.1. Model and Material

The sizing and dimension of the RC beam is exactly the same as the one used in the section 3.2.1 for experimental testing. Moreover, the number and dimension of longitudinal and transversal reinforcements are the same.

For all of the steel reinforcements, B450C steel is used which the properties were shown in table3.5. Although, the concrete grade used here is also similar as the section before, ABAQUS requires the concrete damage plasticity (CDP) data to be given.

In finite element modelling of reinforced concrete structures, it is crucial to represent the nonlinear and anisotropic behavior of concrete with high fidelity. ABAQUS offers a specialized material model called Concrete Damaged Plasticity (CDP) to capture the complex stress-strain relationships and damage mechanisms associated with concrete. This model is widely used in structural engineering simulations due to its ability to simulate both cracking under tension and crushing under compression, along with the progressive degradation of material stiffness.

Concrete behaves differently under tensile and compressive loading. In tension, it exhibits a brittle response, leading to cracking and sudden loss of strength, whereas in compression, it can sustain higher loads with nonlinear plastic deformation before failure. The CDP model accounts for this dual nature by incorporating two separate stress-strain relationships for tension and compression, along with damage parameters that reduce the material stiffness as cracking or crushing progresses. This allows for more realistic simulations of structural elements that experience localized failures, such as bending-induced cracking in beams.

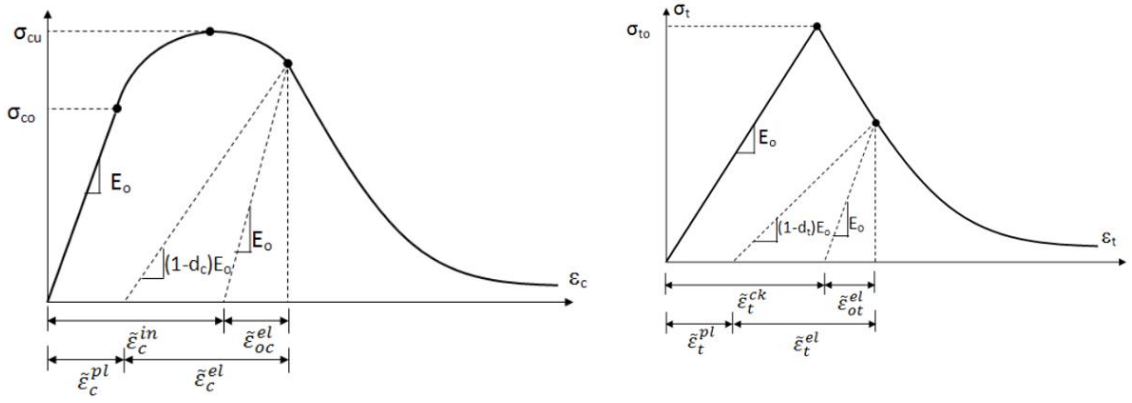

a) Compression b)Tension

Figure 4.1 Stress Strain curve for tension and compression

To effectively utilize the CDP model, ABAQUS requires several input parameters. These include the elastic modulus and Poisson's ratio to define the initial linear elastic response of the material. The tensile and compressive strengths of the concrete are also essential, as they determine the onset of inelastic

behavior. The model then uses tensile and compressive stress-strain data to capture the post-peak softening behavior, which is especially important in replicating crack propagation and energy dissipation in concrete structures.

The young's modulus used for the concrete are obtained based on the Eurocode formulation for concrete under 50MPa strength. Based on the formula 4.1, the obtained young's modulus is 31,475.8MPa.

$$E_{cm} = 22000 \times \left(\frac{f_{cm}}{10}\right)^{0.3} \tag{4.1}$$

Furthermore, the maximum compressive strength of the concrete was obtained from the concrete grade (33MPa) and based on the Eurocode, the maximum tensile strength of the corresponding concrete can be obtained with formula4.2. For the C25/30 concrete, the maximum tensile capacity is 2.56MPa.

$$f_{ctk} = 0.3 \times f_{ck}^{2/3} \tag{4.2}$$

The plastic flow characteristics of the concrete damaged plasticity (CDP) model are defined by several key parameters. One of these is the dilation angle (ψ), which describes the inclination of the plastic potential surface in the p–q stress space under high confinement levels and typically falls within the range of 25° to 40°. Another important factor is the shape parameter (K), representing the ratio of hydrostatic stress on the tensile meridian to that on the compressive meridian under conditions where the maximum principal stress is compressive; a common value used for this ratio is 2/3. Additionally, the biaxial-to-uniaxial compressive strength ratio (σ_{bo}/σ_{co}) is included, with a standard reference value of 1.16 based on literature.

The eccentricity (ε) of the flow potential governs the curvature of the hyperbolic function used to describe the non-associated plastic flow; in most simulations, this parameter is set to a default of 0.1. Another essential component is the viscosity coefficient, which serves to enhance numerical stability and avoid issues such as strain localization or convergence failure. Selecting this value requires careful judgment: overly high values can lead to inaccurate results, while excessively low values may result in computational difficulties. In this study, a viscosity value of 0.0005 was adopted, in alignment with published guidelines. Due to the unavailability of direct experimental calibration data for these parameters, values were sourced from various reliable references in the literature. To ensure the chosen set of parameters did not significantly bias the simulation outcomes, a sensitivity analysis was conducted using ABAQUS. The selected parameters and their sources are outlined in Table 4.1.

Table 4.1 *CDP data*

Dialation Angle(ψ)	Eccentricity (ε)	strength ratio (σbo/σco)	shape parameter (K)	viscosity coefficient
25	0.1	1.16	0.667	0.0005

Moreover, the CDP data regarding the concrete and FRCC are obtained using the ABAQUS CDP Generator software. The principals used in this software are the same what is written in Eurocode and the advantage provided by this software is the ease of use. The inputs of this software are contained of ultimate compressive strength (f_{cu}), ultimate tensile strength (f_{tu}), maximum aggregate diameter (d_{max}) and mesh element characteristics length (l_o). With try and error of the simulation it was obtained that 1 mm mesh element characteristics length provides the most smooth and stable result for this study. The value for d_{max} was also provided in test set up.

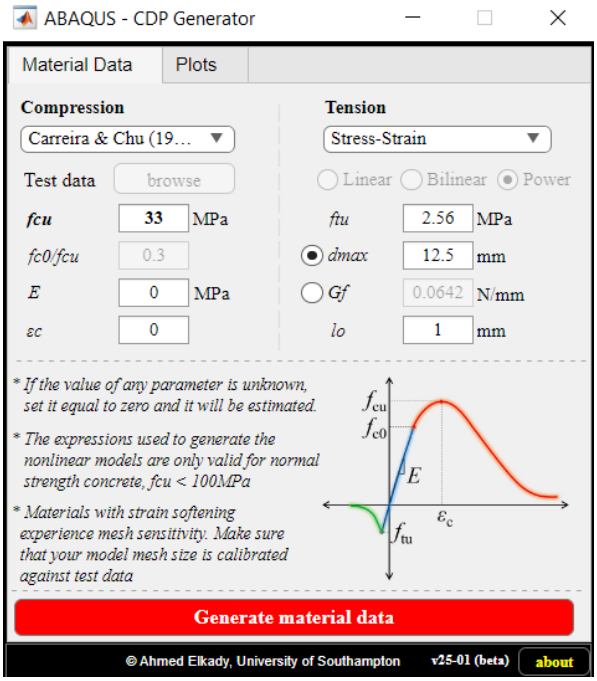

Figure 4.2 ABAQUS CDP Generator software interface

The output of this software is 4 files which provides data for yield stress vs inelastic strain and damage parameter vs inelastic strain for both compression and tension. In table4.2, CDP data for C25/30 concrete in compression is shown and table4.3 illustrates that of tensile properties. The data obtained will be used as the direct inputs for the ABAQUS. **It should be noted that after the material calibration the tensile strength changed from 2.56 to 1MPa.**

Table 4.2 *Compression CDP data*

Compressive yield stress	Inelastic strain	Damage parameter	Inelastic strain
9.9	0	0	0
15.64003	1.1474E-05	0.001752	0.000897
26.03605	0.000125	0.15567	0.002194
30.08715	0.00028	0.507953	0.004847
32.33364	0.000506	0.615933	0.006085
33	0.0007949	0.820907	0.010739
27.8628	0.0021947	0.894362	0.015222
21.283	0.0035516	0.92914	0.019654
16.2375	0.004847	0.934994	0.020758
12.6741	0.0060854	0.952096	0.025167
8.31776	0.008451	0.962941	0.029568
3.48604	0.0152221	0.970301	0.033964

Table 4.3 *Tensile CDP data*

Tensile yield stress	Inelastic strain	Damage parameter	Inelastic strain
1	0	0	0
0.70817	0.016486	0.29182	0.016486
0.51083	0.032973	0.48916	0.032973
0.38174	0.049460	0.61825	0.049460
0.29861	0.065946	0.70138	0.065946
0.24460	0.082433	0.75539	0.082433
0.20800	0.098920	0.79199	0.098920
0.18122	0.115406	0.81877	0.115406
0.15964	0.131893	0.84035	0.131893
0.14070	0.148380	0.85929	0.148380
0.12312	0.164866	0.87687	0.164866
0.10639	0.181353	0.89360	0.181353

4.1.2. Geometry and sections

The whole specimen consists of beam (concrete part), longitudinal reinforcement (tension and compression rebars), transversal reinforcement (stirrups) and supports (half a cylinder steel element). All the parts mentioned are 3D deformable, however, the concrete beam and the steel supports are modelled as the solid elements and the reinforcements are designed as the wire elements. Although, the supports should be designed as rigid bodies for better modelling, the supports in this model are assigned as the steel with high young's modulus which will represents the actual situation with great accuracy and reduce the complexity of the simulation.

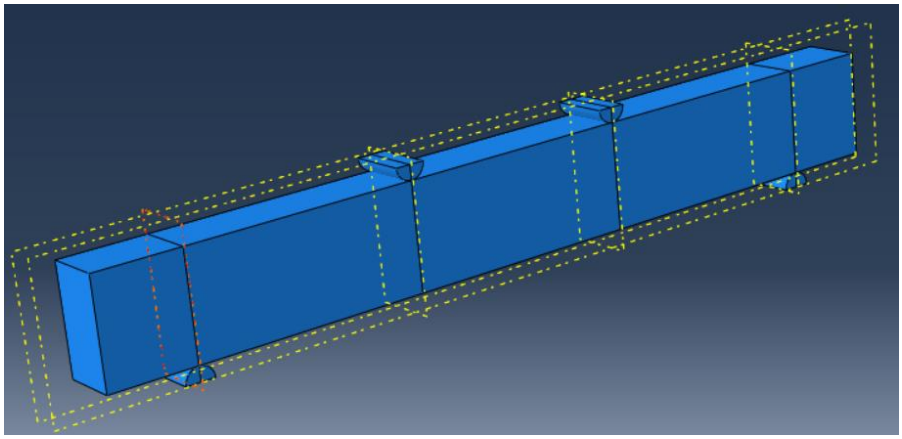

Figure 4.3 Assembled Model

4.1.3. Constitutive Modelling

In the finite element simulation of reinforced concrete beams, the selection of an appropriate analysis step is critical for capturing the complex nonlinear behavior exhibited during loading. In this study, the Static General step available in ABAQUS was employed to model the loading phase of the four-point bending test. This step is well-suited for problems involving progressive loading and material nonlinearity, as it allows for accurate tracking of the response under gradually increasing loads. Unlike dynamic or explicit analysis steps, the Static General step assumes quasi-static conditions, which closely resembles the actual experimental setup where loading is applied slowly and inertial effects are negligible.

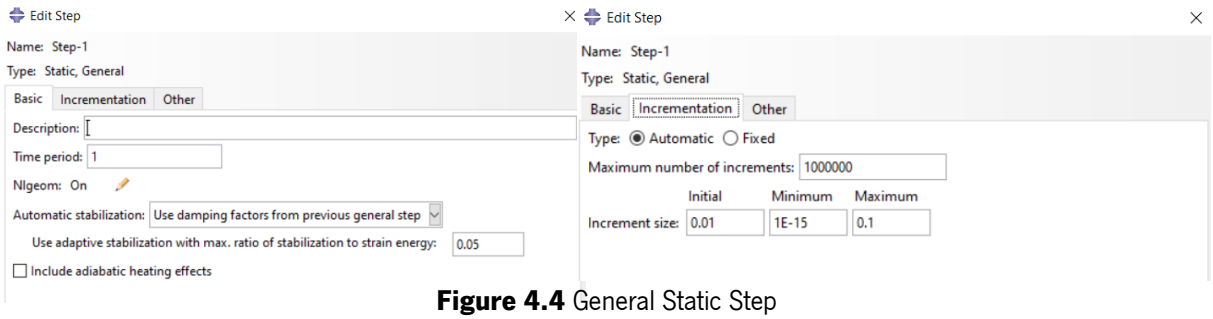

Figure 4.4 General Static Step

An important feature activated in this step is the nonlinear geometry option (NIgeom = ON), which enables the solver to consider geometric nonlinearities such as large deformations and rotations. This is particularly important in the modelling of concrete beams, where significant deflections and crack openings can occur as the load increases, affecting the internal force distribution and overall structural behavior. Enabling this feature ensures that second-order effects, such as stiffness degradation due to deformation, are properly captured in the simulation.

To manage contact behavior within the entire model, a general contact interaction was defined. This approach simplifies the setup process by automatically identifying and applying contact definitions between all surfaces that may come into contact during the simulation. It is particularly useful in complex geometries like RC beams where multiple potential contact pairs may develop, especially as cracking and deformation evolve.

The contact properties for this general interaction were carefully specified to include both normal and tangential behavior. In the normal direction, a "hard contact" formulation was applied, which prevents penetration between surfaces while still allowing separation. This is crucial for simulating the realistic opening of cracks or gaps in concrete when tensile stresses exceed the material's tensile strength.

For the tangential behavior, a penalty friction formulation was used. This method introduces a friction coefficient to simulate the resistance to sliding at the contact interface which has a value of 0.35. The penalty method balances accuracy and numerical stability and is appropriate for quasi-static problems like the four-point bending of concrete beams.

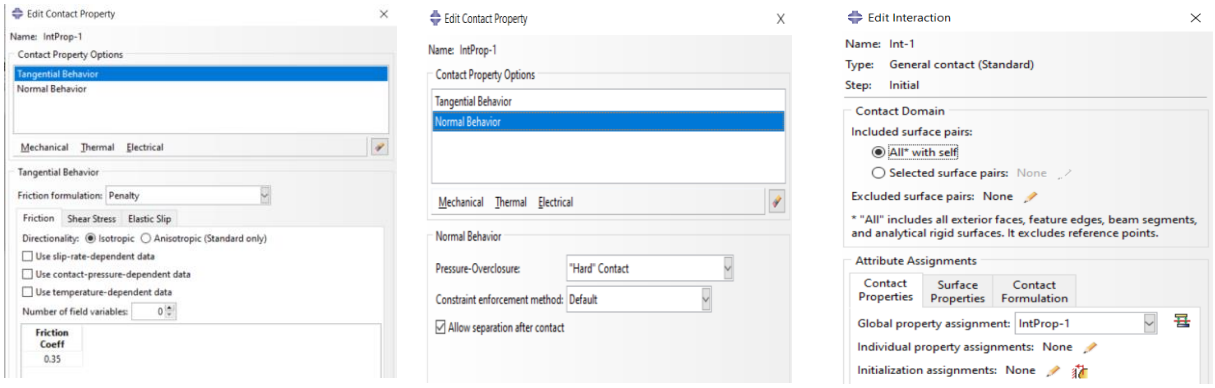

Figure 4.5 Interaction

In addition to contact interactions, embedded region constraints were defined to model the bond between the steel reinforcement and the surrounding concrete matrix. In ABAQUS, the "embedded region" interaction allows one part (the rebar) to be fully contained within another (the concrete host element), enforcing compatibility of displacements without requiring explicit surface-to-surface bonding definitions. This method assumes perfect bond between the two materials, meaning no slip occurs between the rebar

and concrete during loading. This simplification is widely accepted in structural modelling unless bond-slip behavior is being specifically investigated.

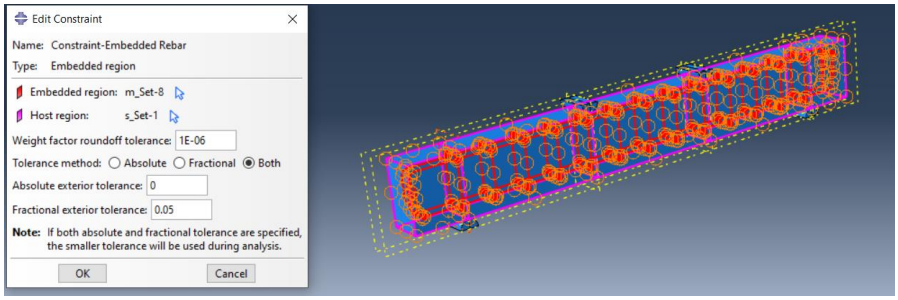

Figure 4.6 Embedded region constraints

Together, these interaction definitions ensure a comprehensive and realistic representation of material interactions during loading. They form a critical foundation for accurately capturing crack initiation, load transfer mechanisms, and failure progression in the RC beam model.

4.1.4. Mesh and Boundary Condition

To represent the support conditions, the bottom surfaces of the two support rollers were constrained in the vertical (Y) direction, effectively preventing any downward or upward movement. This setup mimics the real-world support where the beam rests on two roller bearings, allowing free horizontal movement (X-direction) while restraining vertical displacement. No constraints were applied in the X-direction to the supports, allowing for the natural expansion or contraction of the beam.

For the loading mechanism, a vertical displacement was applied to the top surfaces of the loading plates, positioned symmetrically between the supports to create a four-point bending scenario. Rather than applying a force, a prescribed displacement was used, which provides better control over the simulation, especially when dealing with nonlinear behavior such as cracking, strain localization, and post-peak softening. This method also improves convergence and stability in the simulation, particularly near the ultimate load and failure zones.

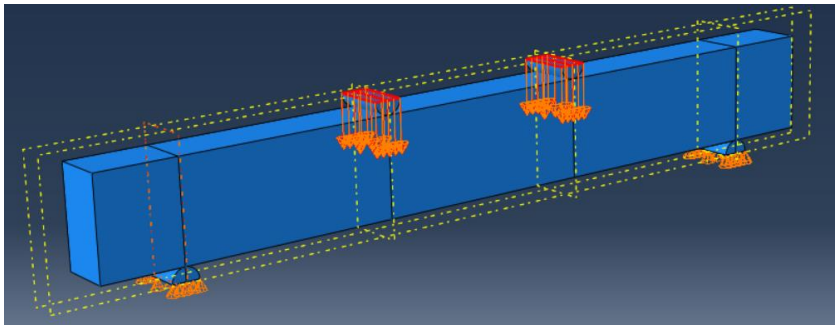

Figure 4.7 Boundary Conditions and Loading

Following the modelling with mesh section, the concrete beam and steel support was discretized using C3D8R elements—eight node linear brick elements with reduced integration and hourglass control. These elements are widely used in nonlinear simulations involving solid structures due to their ability to capture three-dimensional stress states, cracking, and crushing behavior of concrete. The reduced integration scheme significantly improves computational efficiency while maintaining sufficient accuracy, especially when the mesh is adequately refined. These elements are particularly effective for simulating concrete's complex nonlinear behavior.

For the longitudinal reinforcement bars—both tension and compression rebars— and transversal reinforcement (stirrups) the T3D2 element type was employed. These are two-node linear 3D truss elements that carry axial force only. Since reinforcement bars are typically modelled as 1D elements embedded within the 3D concrete domain, the T3D2 formulation is appropriate. It allows for the efficient simulation of rebar contribution to the flexural and axial resistance of the beam without unnecessarily increasing the model complexity or computation time. These elements were embedded into the concrete mesh using the embedded region constraint to simulate perfect bond between steel and concrete. The final configuration of the mesh assembly is shown in figure4.8.

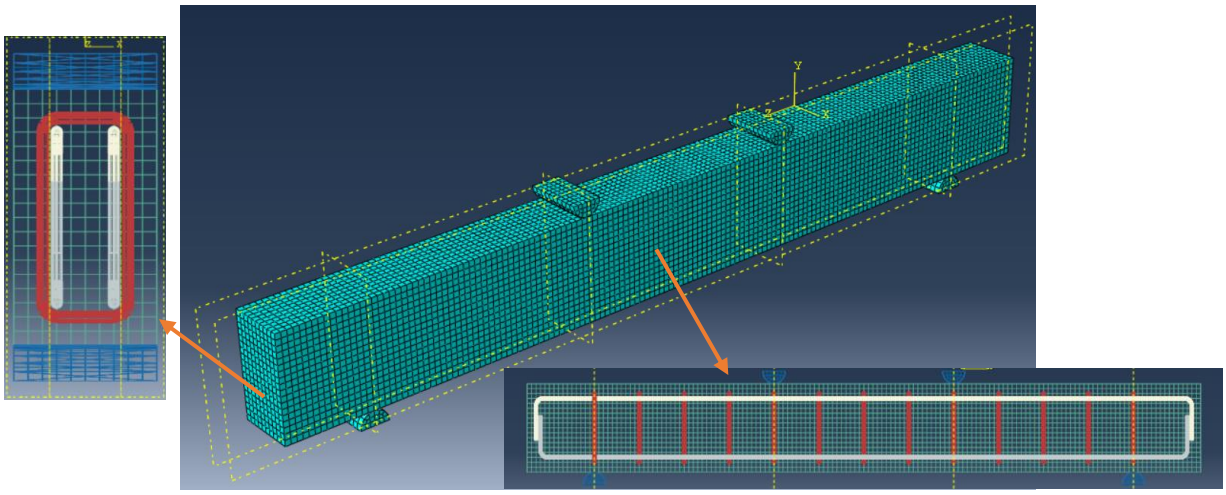

Figure 4.8 Mesh

4.1.5. Results

The results of this study are assessed through a direct comparison between experimental data and the outcomes derived from numerical simulation. This comparison not only validates the numerical model but also provides a deeper understanding of how mesh density influences the accuracy of the results.

From the figure4.9, it can be seen that the numerical model demonstrates a strong correlation with the experimental behavior, particularly in the initial elastic and peak load regions. Both mesh configurations

successfully reproduce the general flexural response of the beam, confirming the accuracy of the modeling approach and material definitions. The coarse mesh slightly underestimates the peak load but captures the post-peak plateau with greater stability. In contrast, the fine mesh provides a closer approximation to the peak response, though it shows a slightly sharper post-peak decline.

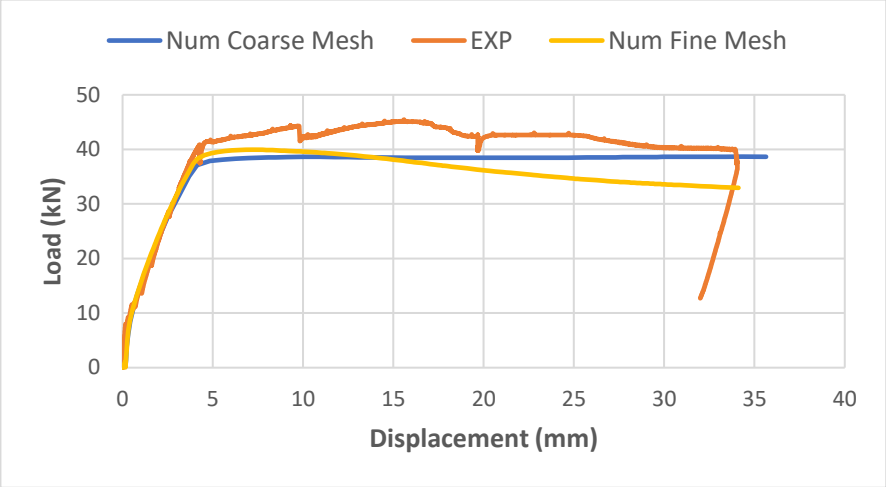

Figure 4.9 Load vs Displacement of RC beam

Figure4.10 a) displays the tensile damage distribution across the beam. Here, the damage is predominantly concentrated in the lower central region between the two loading points, indicating the development of flexural cracks. This pattern is consistent with the expected behavior of reinforced concrete beams under bending, where the bottom fiber experiences tension due to flexure. The symmetrical spread of the tensile damage also suggests a uniform distribution of bending stress along the beam's span.

Figure4.10 b) illustrates the compressive damage profile. As seen in the figure, the upper central region of the beam exhibits noticeable compressive degradation. The red and yellow zones along the top edge of the beam confirm localized crushing and material degradation due to high compressive stresses. This is also in agreement with the failure mechanism of concrete, where concrete crushing typically occurs at the top fibers when the beam is subjected to downward loading.

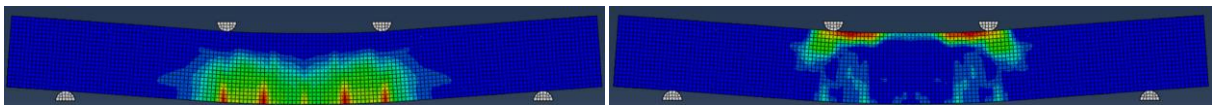

a) Tensile Damage b) Compression Damage

Figure 4.10 Damage Contours

Moreover, after calibration of the model with experimental data, young's modulus value changed to 34,000MPa from 31,475.8MPa for the corresponding concrete. Also the maximum tensile capacity was also changed to 1MPa after model calibration. This decrease in the tensile capacity can be due to the

poor casting quality or other factors such as curing condition, environmental condition and bond deficiencies affecting the experimental testing.

4.2. Material Characterisation

In the subsequent phase of the numerical investigation, a three-point bending test was modeled using ABAQUS to simulate the structural response of the specimen under flexural loading. This simulation was designed to replicate the actual experimental setup and boundary conditions in order to provide a reliable basis for comparative analysis. The primary goal of this simulation is to calibrate the tensile strength parameter of the FRCC 2.1% material model by matching the numerical load–displacement response with that obtained from experimental testing. Given the significant sensitivity of flexural behavior to the tensile characteristics of the material, accurately estimating the tensile strength is critical for achieving a validated and predictive numerical model. Therefore, an iterative procedure was followed, in which the input tensile strength was adjusted and the resulting numerical response was evaluated against the experimental curve until a satisfactory agreement was reached.

4.2.1. FRCC Damage Data

The tensile stress–strain response of FRCC exhibits significant differences from that of conventional concrete, particularly in the post-peak region. In conventional concrete, the tensile capacity reaches its maximum at peak stress, after which a sharp and rapid degradation in tensile strength occurs due to the brittle nature of the material. Once microcracks initiate and propagate under increasing tensile load, the concrete matrix lacks internal mechanisms to arrest or redistribute these cracks. As a result, the post-peak region of the stress–strain curve shows a steep decline, and the residual tensile strength approaches zero at failure. This behavior reflects the inherent brittleness and low energy absorption capacity of plain concrete under tension.

In contrast, FRCC materials exhibit a much more ductile behavior due to the presence of discrete reinforcing fibers distributed within the matrix. After reaching the peak tensile strength, the stress–strain curve of FRCC shows a moderate drop—typically around 30%—followed by a plateau-like behavior where tensile strength is maintained at a nearly constant level until failure. This sustained tensile resistance is attributed to the bridging action of the fibers across microcracks. As cracks initiate and open, fibers continue to transfer tensile forces, delaying the localization of strain and preventing catastrophic failure. This post-cracking behavior results in a more stable and ductile fracture process. The enhanced post-

peak tensile behavior of FRCC improves ductility, crack control, and residual strength, leading to greater energy absorption, durability, and structural resilience—making it a superior and more sustainable alternative to conventional concrete.

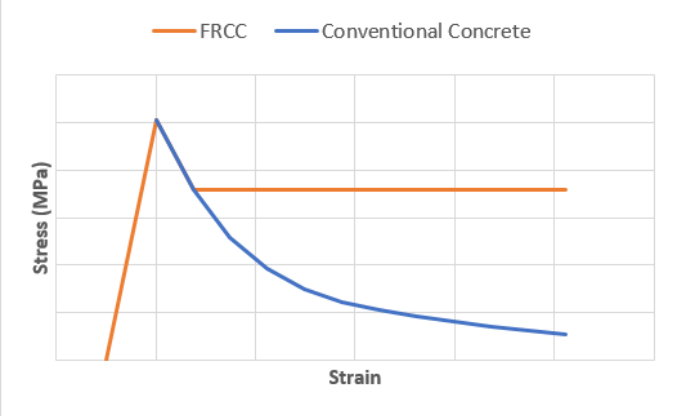

Figure 4.11 Tensile strength schematic for FRCC and Concrete

4.2.2. Geometry, Material and overall Modelling

As it was mentioned in the section3.1.1, the cross section of the specimen is 40 × 40 mm and the length of the specimen is 160mm. In this specimen there is no reinforcement and the material is pure FRCC2.1% due to the fact that this test is performed in order to obtain material properties of the material.

The step and interactions used in this simulation are similar to the one used in the four point bending test of the bare beam, however, due to the fact that there is no reinforcement used in the specimens, embedded region constrain was not used. Mesh elements are all C3D8R as a results of all 3D elements. Loading and boundary conditions are exactly the same with the four point bending simulation with one slight difference that the loading body (the surface which the displacement is being applied instead of loading) is a single half a cylinder instead of two. The rest of the setup is similar between three point bending and four point bending and discretized view of the simulation is shown in figure4.12.

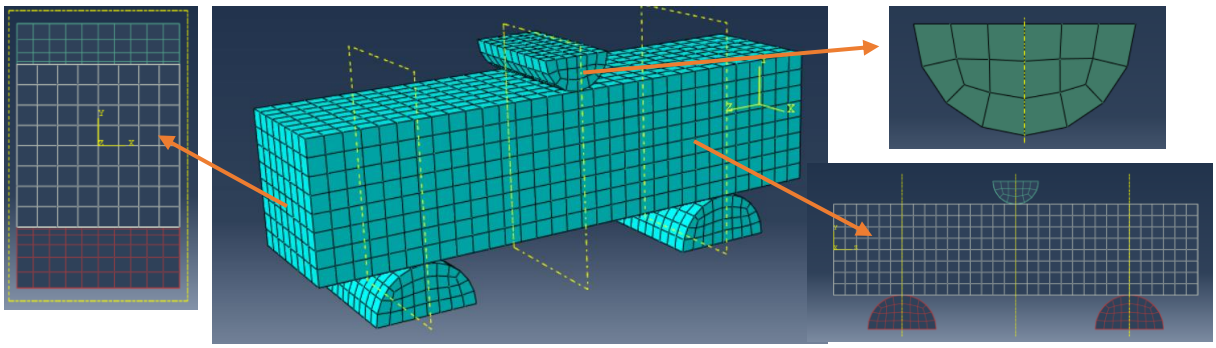

Figure 4.12 Mesh

4.2.3. Results

Figure 4.13 presents the load–displacement response obtained from the numerical simulation of the three point bending test for the FRCC 2.1% specimen, alongside the experimental results of three repeated tests (Test 1, Test 2, and Test 3). In this simulation, the compressive strength of the FRCC mix was set to 71.5 MPa, as determined from experimental testing detailed in Section 3.1.3. The tensile strength, which was the primary unknown parameter in this modeling phase, was identified through an iterative calibration process. After multiple simulation runs and adjustments, **a tensile strength value of 6 MPa yielded a numerical response that closely matched the experimental behavior**. As shown in the graph, the numerical curve lies approximately between the three experimental curves, representing an average response in terms of both peak load and post-peak softening behavior. Although minor discrepancies are observed in the post-peak region, the overall agreement confirms the validity of the selected tensile strength. The numerical curve effectively captures the flexural behavior and provides an acceptable approximation of the material's actual performance.

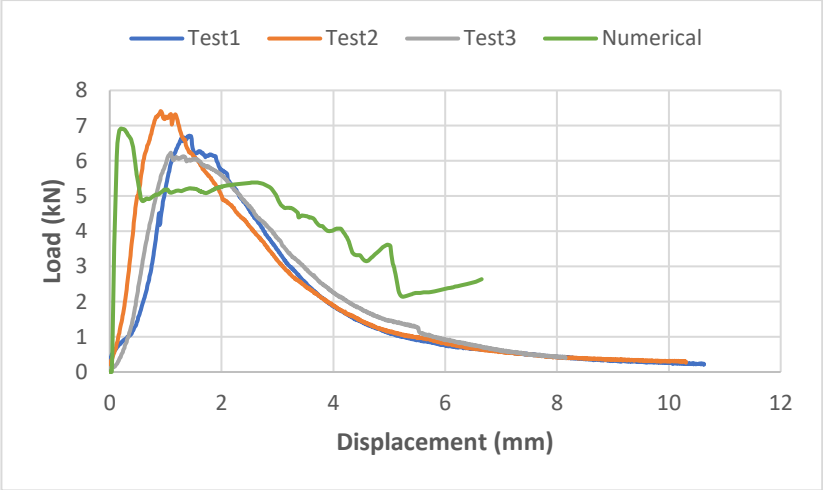

Figure 4.13 Load vs Displacement FRCC 2.1%

4.3. Beam Testing Validation and Calibration for FRCC

At this section, the FEM of the beams under four point bending test are analysed. The modelling process of the beams are similar as what was done in the section 4.1 for the bare beam with one slight difference that in addition to the bare beam, there is a new layer of FRCC reinforcement. This layer is implemented as a substitution for the concrete cover in some sides and it has two distinct configurations. Bottom reinforcement and U-jacketing are two different shape of FRCC reinforcement that are added to the

beams. These configurations will have various thicknesses and different materials that will be deeply discussed in the following.

4.3.1. 1.1% Fiber ratio

The reinforcement material used in this test is the FRCC which consist of 1.1% of steel fibers. The experimental results of the same beam reinforced with U-jacketing of the same material is present due to some previous works of experimental test campaign. As a result, firstly the tensile strength of the FRCC 1.1% is calibrated with load vs displacement results that was obtained and following that, the bottom reinforcement with same thickness and same material was modelled on the beam to observe the differences between two configurations. The thickness of the reinforcement in both are configurations is 20 mm which was implemented on the beam after the concrete cover was removed. Moreover, the compressive strength of this material is 98 MPa which was obtained from previous tests of the experimental test campaign.

After proceeding with the iterative process in order to obtain the tensile strength of the FRCC1.1%, maximum tensile strength was derived as 5 MPa. Following that, both configurations with the same thickness are modelled with the finalized tensile strength and results are shown in figure4.14. It should be noted that the experimental results of bottom reinforcement FRCC 1.1% is not available and the numerical results are shown as a comparison between two configurations.

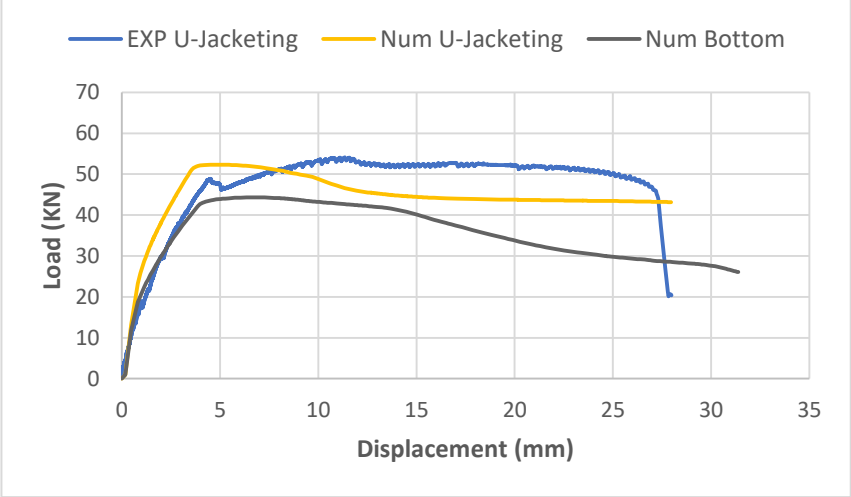

Figure 4.14 Load vs Displacement FRCC 1.1%

Figure 4.14 presents the load–displacement response of the U-jacketed beam strengthened with FRCC 1.1%, comparing experimental results with those of the numerical simulation. The close agreement between the experimental and numerical U-jacketing curves, particularly in terms of initial stiffness, peak load (54 kN and 53 kN), and general post-peak trend, validates the accuracy of the FE model. This

confirms that the selected material properties, including the tensile strength of 5 MPa obtained from earlier iterative calibration, reliably simulate the behavior of FRCC in structural applications.

Also included in the figure is the numerical simulation of the beam with FRCC reinforcement applied only at the bottom. This curve shows a notably lower peak load of 44 kN and a more pronounced post-peak degradation. This contrast highlights the superior performance of the U-jacketing technique, which offers better confinement, crack control, and energy dissipation through multidirectional FRCC engagement, compared to the limited effect of bottom-only reinforcement.

4.3.2. 2.0% Fiber ratio

Similar modelling and procedure was conducted for the beam with FRCC 2% as the reinforcement material. As a result of iterative procedure, the tensile strength was obtained as 8MPa with 30% decrease in the post peak area up to failure. The load vs displacement curve both bottom and U-jacketing are shown in figure4.15. The graph compares results of calibrated FRCC 2% material properties, firstly with the experimental results and secondly, the differences between two configurations. Moreover, the compressive strength of this material is 98 MPa which was obtained from previous tests of the experimental test campaign.

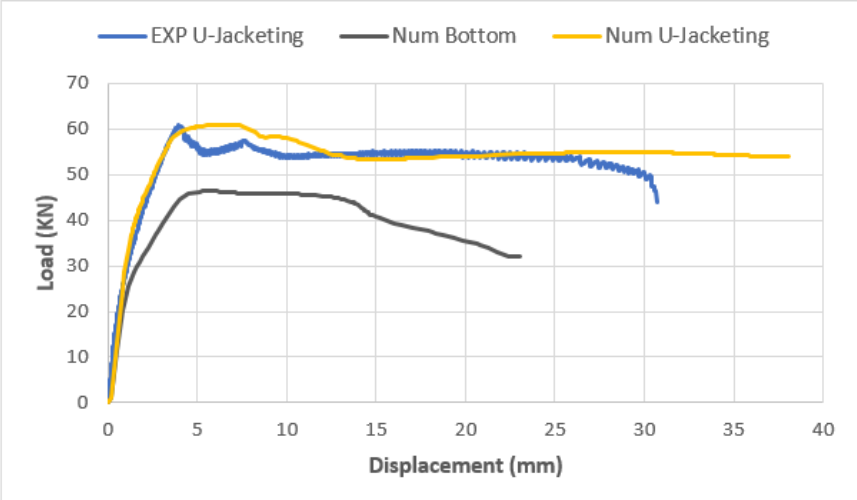

Figure 4.15 Load vs Displacement FRCC 2%

Figure 4.15 displays the load–displacement curves of the U-jacketed beam reinforced with FRCC 2%, including both experimental and numerical results, along with the numerical response of the bottom-reinforced beam. The numerical U-jacketing curve aligns well with the experimental data in terms of peak load of 61 kN, initial stiffness, and post-peak behavior, further confirming the reliability of the FE model in simulating the FRCC material and calibration of the tensile property.

Compared to the bottom reinforcement, which reached a peak load of approximately 47 kN and experienced a more rapid degradation in strength, the U-jacketing configuration clearly provides enhanced structural performance. The experimental U-jacketing specimen maintained a nearly constant load level beyond the peak displacement, which reflects the strain-hardening and crack-bridging capabilities of FRCC 2% under flexural loads.

The increase in fiber content from 1.1% to 2% contributed to higher ductility, improved energy dissipation, and a more gradual post-peak softening response. This validates the role of fiber dosage in promoting residual tensile strength and delaying failure, particularly when employed in a confinement-oriented configuration like U-jacketing.

4.3.3. 2.1% Fiber ratio

The material used in this simulation is a combination of 1.1% steel fibers and 1% PE fibers. Unlike the previous materials that the experimental result was present only for U-jacketing, FRCC 2.1% results are obtained in section 3.2.3 for both configurations. As previously discussed, the tensile strength of the material was obtained with DIC analysis and material characterisation test. Both of the previous methods derived the tensile strength around 6MPa, however, the iterative process was also implemented here to compare the results. Based on both configurations, the tensile strength obtained is 8MPa which is higher than previous approaches. As a result, the numerical modelling results for both values for tensile strength (6 and 8 MPa) will be demonstrated in the following.

Based on the experimental testing, the thickness of bottom reinforcement was around 50mm which is higher than the expected thickness. This variation is due to the fact that removing the concrete cover and also adding the FRCC layer with desirable thickness, is a difficult task to be done precisely. As a result, these variations occur. On the other hand, the U-jacketing has 30 mm thickness on the bottom part and 20mm thickness on the sides. All of the FRCC thicknesses can be seen in figure4.16.

a) Bottom reinforcement

b) Bottom part of U-jacketing

c) Sides of the U-jacketing

Figure 4.16 FRCC 2.1% thickness

Consequently, the load vs displacement results of the beams with FRCC 2.1% bottom reinforcement is shown in figure4.17. In the initial phase of loading up to 5 mm displacement, all curves display similar stiffness, indicating good agreement in the elastic range. This suggests that the material properties prior to cracking were accurately defined in both numerical models.

As the load increases and the beam enters the post-cracking regime, divergence between the curves becomes evident. The experimental peak load is approximately 57 kN at a displacement of around 11 mm. The numerical simulation with 8 MPa tensile strength closely reproduces both the magnitude and shape of the experimental curve, including the peak load and post-peak plateau. In contrast, the 6 MPa model underestimates the peak strength and shows reduced load capacity in the post-peak region, failing to fully capture the tensile strain-hardening effect observed in the experiment.

The experimental response demonstrates a stable plateau with gradual softening, maintaining significant load-carrying capacity up to failure at approximately 38 mm displacement. This ductile behavior is well reflected in the 8 MPa numerical model, which also shows sustained load after the peak.

Overall, the comparison indicates that the iteratively calibrated tensile strength of 8 MPa provides a more accurate representation of the actual performance of the FRCC 2.1% system within the RC beam. Although the 6 MPa value was experimentally derived from DIC and direct tests, it underestimates the structural response. This emphasizes the importance of using both experimental data and numerical calibration in defining effective material properties for structural simulations.

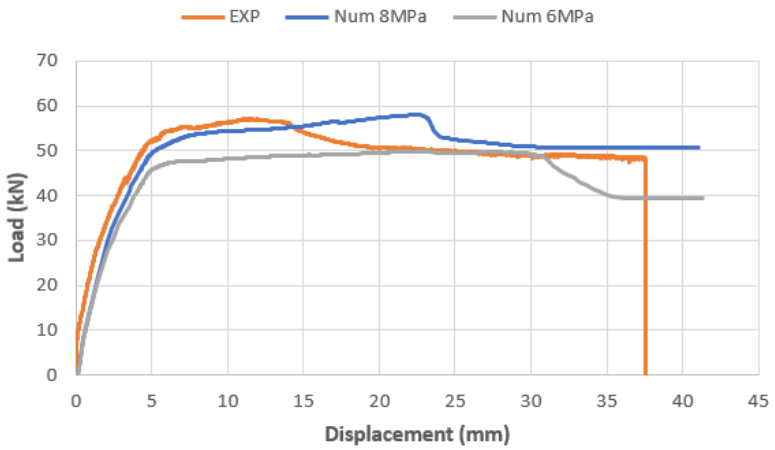

Figure 4.17 Load vs Displacement FRCC 2.1% Bottom reinforcement

Following that, the load vs displacement results of the beams with FRCC 2.1% U-jacketing is shown in figure4.18. In the elastic range up to 5 mm displacement, all curves demonstrate similar stiffness, indicating that both numerical models capture the uncracked behavior accurately. This agreement

confirms the appropriateness of the adopted elastic material properties for concrete, reinforcement, and FRCC in the finite element model.

The experimental specimen reaches a peak load of approximately 54 kN at around 7 mm displacement, followed by a plateau region and gradual softening. The numerical model with 8 MPa tensile strength effectively captures this peak load and the subsequent strain-hardening behavior, closely matching the overall trend of the experimental curve. In contrast, the 6 MPa model under predicts the load-carrying capacity and exhibits a less pronounced post-cracking response, indicating insufficient tensile contribution from the FRCC layer when a lower tensile strength is assumed.

The experimental response beyond the peak is characterized by a relatively stable plateau, maintaining load levels above 48 kN up to failure at approximately 40 mm displacement. This ductile behavior is effectively captured by the 8 MPa numerical model, which continues to show stable load resistance in the post-peak regime. Minor fluctuations observed in the numerical curve are attributed to localized strain effects and numerical convergence during large deformations. In contrast, the 6 MPa model shows early degradation of load capacity after peak, with a steady decline starting shortly after cracking.

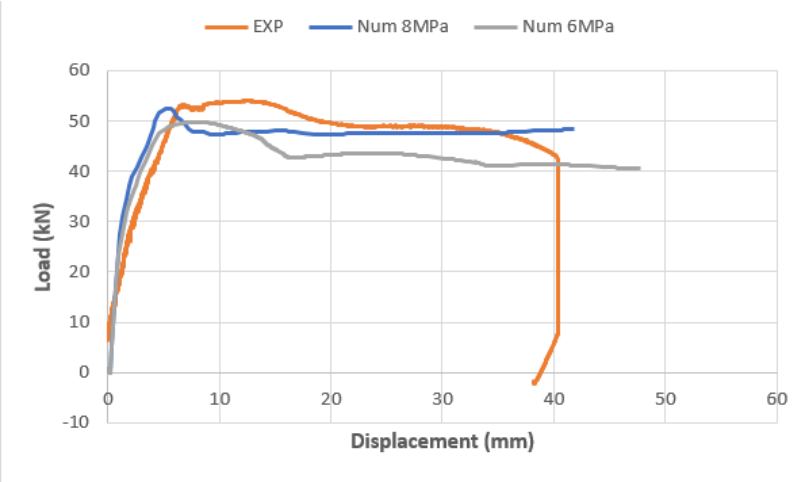

Figure 4.18 Load vs Displacement FRCC 2.1% U-jacketing

4.4. Full Scale Beam (Parametric Study)

Following the successful calibration and validation of the numerical models with scaled experimental data, a parametric study was conducted to assess the structural performance of the proposed strengthening techniques in full-scale applications. Unlike previous simulations, which employed reduced dimensions for practical testing constraints, this study investigates the behavior of full-sized structural elements to provide more accurate insights into real-world performance.

The full-scale reinforced concrete beam modelled in this study has a total length of 5100 mm and a rectangular cross-section measuring 500 mm in height and 300 mm in width. A concrete cover of 35 mm is applied to protect the reinforcement from environmental effects and ensure durability. The internal reinforcement configuration consists of three longitudinal bars with a diameter of 14 mm placed in the upper (compression) zone, and four longitudinal bars with a diameter of 18 mm placed in the lower (tension) zone of the beam section, conforming to standard structural detailing practices. Moreover, the transverse reinforcement used are 8 mm thick and the spacing is 100 mm between each stirrups.

Two external strengthening strategies are examined: bottom reinforcement and U-jacketing, both applied with a uniform thickness of 35 mm. These techniques are evaluated for their contribution to load-bearing capacity, ductility, and failure behavior of the beam under flexural loading.

This parametric study is intended to evaluate the structural efficiency and applicability of the selected strengthening methods when scaled to real dimensions, thereby supporting the development of robust retrofitting solutions for existing concrete infrastructure.

The modelling procedure is exactly same as the FEM of four point bending test with one slight different that the double symmetry (xy and yz plane) boundary conditions is used in order to reduce the computational cost. For the easier modelling of the upper longitudinal reinforcement, one of the 14mm rebars is converted to two 7mm rebars.

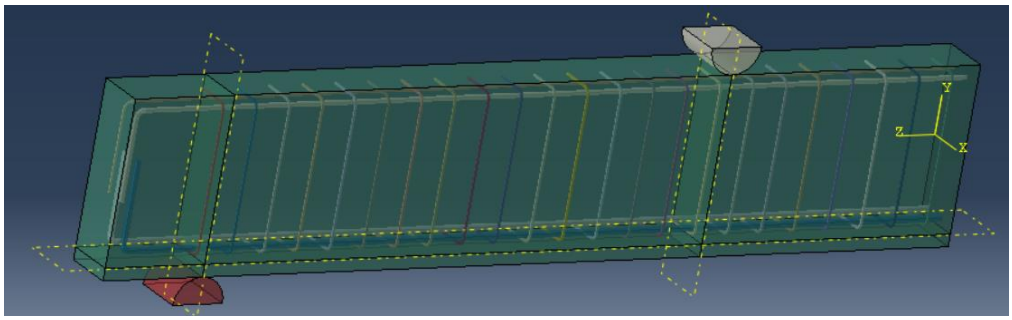

Figure 4.19 Full scale beam

4.4.1. Bare Beam Analysis

At the beginning, the RC beam without any strengthening is modelled and also the effect of using symmetry boundary condition was investigated. As it can be seen in the figure 4.20, the symmetry boundary condition does not affect the result notably and as it reduces the computational cost significantly, it does not decrease the accuracy, as a result, the rest of the full scale analysis is conducted with symmetry boundary condition.

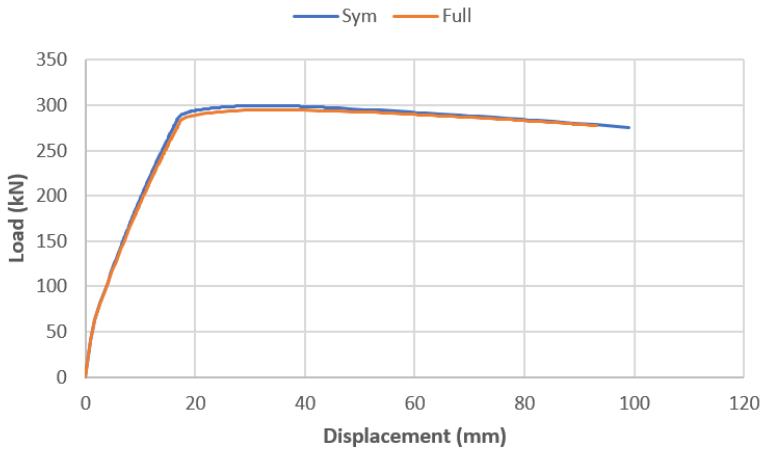

Figure 4.20 Bare Beam Analysis

4.4.2. FRCC Tensile Property

The first phase of the parametric study focuses on investigating the influence of FRCC tensile strength on the flexural behavior of full-scale reinforced concrete beams strengthened with U-jacketing and bottom reinforcement techniques. In this analysis, the geometry and internal reinforcement layout of the beam remain constant, while the tensile strength of the FRCC used for strengthening is varied.

To capture a broad range of material behavior, five distinct tensile strength values were considered: 5 MPa, 7.5 MPa, 10 MPa, 12.5 MPa, and 15 MPa. These values encompass both conservative and high-performance FRCC material characteristics, allowing for a comprehensive understanding of how tensile capacity affects overall load-bearing behavior.

Each configuration was simulated under the same loading and boundary conditions, with results evaluated in terms of load-displacement response, peak load capacity, stiffness, post-peak ductility and the percentage of increase in flexural capacity in comparison with the bare beam. This variation provides insight into the sensitivity of structural performance to the tensile strength of the FRCC material and helps in optimizing the material selection for retrofit applications. Furthermore, by analysing both U-jacketing and bottom reinforcement schemes across these tensile strength values, the study aims to determine whether enhanced tensile strength translates proportionally into improved performance and to what extent the effectiveness of each strengthening strategy is influenced by the FRCC material properties.

The results shown in Figure 4.21 present the influence of FRCC tensile strength on the load-displacement behavior of full-scale reinforced concrete beams strengthened using two different techniques: bottom reinforcement (left) and U-jacketing (right). Each curve represents a beam strengthened with FRCC

material having a different tensile strength (5, 7.5, 10, 12.5, and 15 MPa), in comparison with an unstrengthened "Bare" beam.

- Bottom Reinforcement (a):

Increasing the FRCC tensile strength leads to a progressive enhancement in peak load capacity and however, the improvement is relatively modest but consistent, with load capacity increasing from approximately 300 kN (bare) to around 370 kN for the 15 MPa case. Moreover, the post-peak slope shows gradual softening across all cases, indicating stable ductile behavior.

- U-Jacketing (b):

The impact of FRCC tensile strength is much more pronounced in the U-jacketing configuration. Also, with the increase from 5 MPa to 15 MPa, there is a substantial gain in both load capacity and ductility. The peak load rises from 300 kN (bare) to over 420 kN with 15 MPa FRCC which demonstrates the greater confinement and flexural enhancement provided by the U-jacketing system.

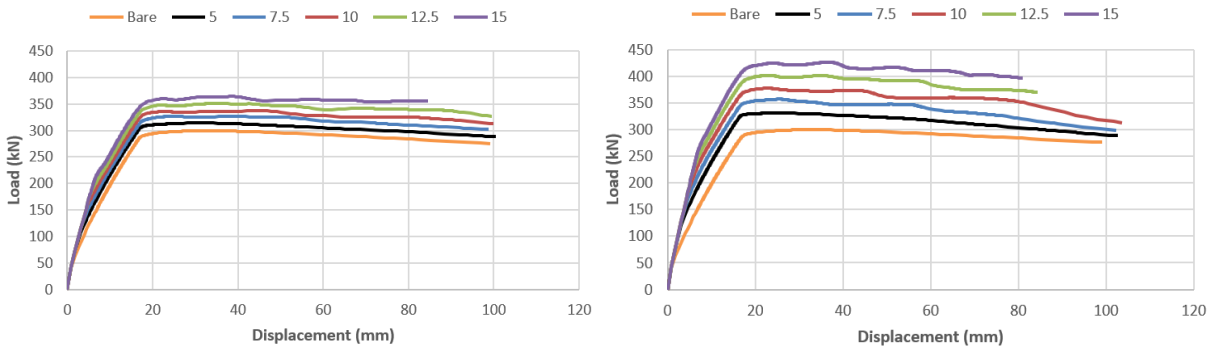

a) Bottom Reinforcement b) U-Jacketing

Figure 4.21 Load vs Displacement for distinct tensile strengths

Figure 4.22 shows how the flexural capacity of reinforced concrete beams improves as the tensile strength of the FRCC material increases, comparing two different strengthening methods: bottom reinforcement and U-jacketing. As the tensile strength of the FRCC increases, both methods lead to better performance, but not to the same extent.

In the case of bottom reinforcement, the increase in flexural capacity is gradual. With an FRCC tensile strength of 5 MPa, the flexural strength improves by about 4.85%, and as the tensile strength reaches 15 MPa, the increase goes up to around 21.56%. This trend clearly shows that stronger FRCC enhances the contribution of the added layer at the bottom, but the effect is limited since the reinforcement is concentrated only on one face of the beam.

U-jacketing, on the other hand, shows a much more significant impact. Starting from a 9.36% increase at 5 MPa, the flexural capacity rises sharply to over 40% when the FRCC tensile strength reaches 15 MPa. This is because the U-jacketing setup wraps around the beam sides as well, providing better confinement and engaging more of the beam cross-section. As a result, the material can better resist cracks and distribute stress, leading to a much stronger overall response

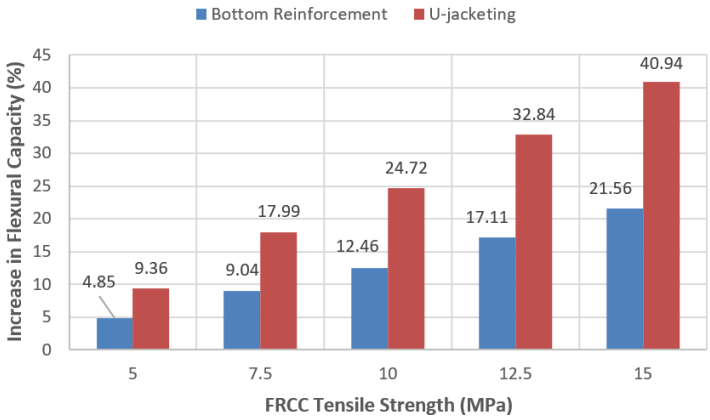

Figure 4.22 Increase percentage in flexural capacity with raising the FRCC tensile strength

4.4.3. Concrete Grade

The second stage of the parametric study examines the influence of concrete grade on the flexural performance of full-scale reinforced concrete beams strengthened with FRCC-based techniques. While the existing concrete grade C25/30 used in experimental and numerical validation had a compressive strength of 33 MPa, the parametric study expands the scope to include a broader range of concrete grades to assess their impact on global structural behavior.

The selected compressive strength values include 15 MPa, 20 MPa, 25 MPa, 33 MPa, and 38 MPa, representing low to moderately high-strength concrete typically encountered in practical applications. With each variation in compressive strength, corresponding material properties such as the elastic modulus and tensile strength were also updated, following the empirical formulations 4.1 and 4.2. All the properties are provide in table 4.4. These property adjustments ensure that the simulation accurately reflects changes in the mechanical behavior of the concrete core material. Both bottom reinforcement and U-jacketing strengthening schemes were analysed under each concrete grade to evaluate their compatibility and performance sensitivity to varying substrate strength.

Table 4.4 *Concrete mechanical Properties*

Compressive Strength (Mpa)	Tensile Strength (Mpa)	Young's modulus (Mpa)
15	1.82	24845.63
20	2.21	27085.18
25	2.56	28960.41
33	3.08	31475.81
38	3.21	32036.35

The load–displacement responses presented in Figure 4.23 demonstrate the significant influence of concrete grade and the applied strengthening techniques on the structural behavior of full-scale RC beams. Each subfigure illustrates the load–displacement behavior for a different strengthening configuration: (a) bare beam, (b) bottom reinforcement, and (c) U-jacketing, with five different concrete grades ranging from 15 MPa to 38 MPa.

In the bare beam configuration (Figure 4.23a), increasing the concrete compressive strength leads to a clear enhancement in flexural capacity. Beams with higher concrete grades (33 MPa and 38 MPa) exhibit superior load-bearing performance compared to those with lower strengths (15 MPa and 20 MPa). This trend reflects the direct contribution of the concrete core in resisting compressive stresses during bending. However, despite the increase in peak load, the structural performance remains limited by the absence of external reinforcement, emphasizing the need for effective strengthening measures in full-scale applications.

The bottom reinforcement configuration (Figure 4.23b) shows notable improvements in load capacity. Compared to the bare beam, this method enhances the load-carrying capacity by introducing a layer of FRCC at the tension face, effectively increasing the section's moment resistance. The beams strengthened with bottom reinforcement and higher concrete grades (33 MPa and 38 MPa) demonstrate the highest flexural capacities among the group. This synergy between the high-performance FRCC layer and the improved substrate material illustrates the benefits of targeted reinforcement along the tension zone of the beam.

In the U-jacketing configuration (Figure 4.23c), the structural enhancement is the most significant among all cases. U-jacketing not only reinforces the tension zone but also provides lateral confinement and shear resistance through its side components. Across all concrete strengths, U-jacketed beams display the highest load capacities, with the 38 MPa beam achieving the maximum value. The consistent improvement in performance across the range of concrete grades suggests that U-jacketing is less

sensitive to the base material properties due to its comprehensive confinement mechanism and increased section stiffness.

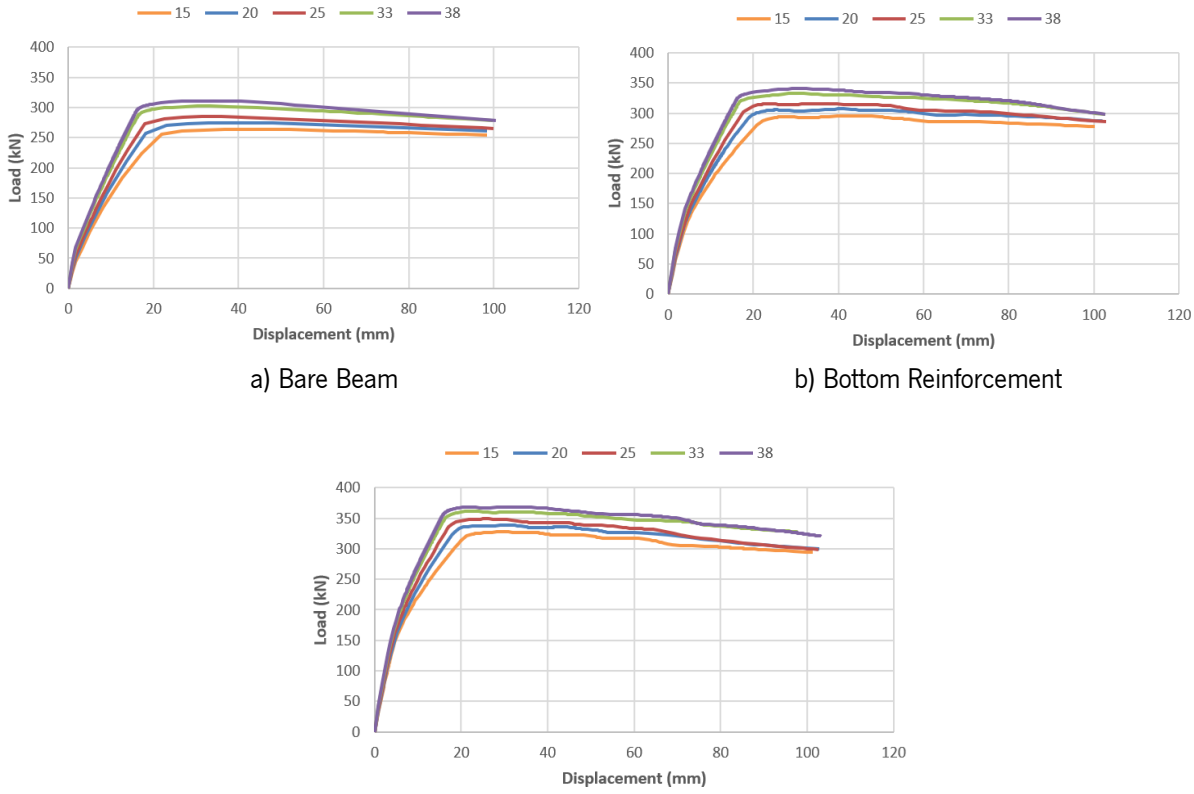

a) Bare Beam

b) Bottom Reinforcement

c) U-jacketing

Figure 4.23 Load vs Displacement for distinct Concrete Grades

The bar chart in Figure 4.24 presents the percentage increase in flexural capacity of reinforced concrete (RC) beams strengthened using two different FRCC-based methods—bottom reinforcement and U-jacketing—across a range of concrete compressive strengths (15 MPa to 38 MPa). The results indicate that both strengthening techniques exhibit a clear dependency on the grade of the existing concrete substrate, with notable variations in performance enhancement.

Starting with the U-jacketing method, it consistently demonstrates superior performance compared to bottom reinforcement across all concrete grades. At the lowest concrete strength of 15 MPa, U-jacketing leads to a substantial 24.06% increase in flexural capacity. However, as the concrete grade increases, the percentage gain from this method gradually declines, reaching 18.55% at 38 MPa. This trend suggests that the relative effectiveness of U-jacketing is more pronounced in weaker substrates, where the additional confinement and tensile resistance provided by the FRCC material contribute significantly to structural performance. As the base concrete becomes stronger, the system's reliance on external strengthening diminishes, resulting in lower proportional gains.

In contrast, the bottom reinforcement technique shows a similar downward trend but with markedly lower flexural improvements. The maximum increase in flexural capacity with this method is 11.88% at 15 MPa

and drops to 9.51% at 38 MPa. The smaller difference in percentages between concrete grades for this method implies that bottom reinforcement offers a more uniform but less impactful enhancement, likely because it contributes directly to tensile capacity with limited effect on compression or shear zones. Additionally, the modest variation with increasing concrete strength highlights that this method is less sensitive to substrate quality compared to U-jacketing.

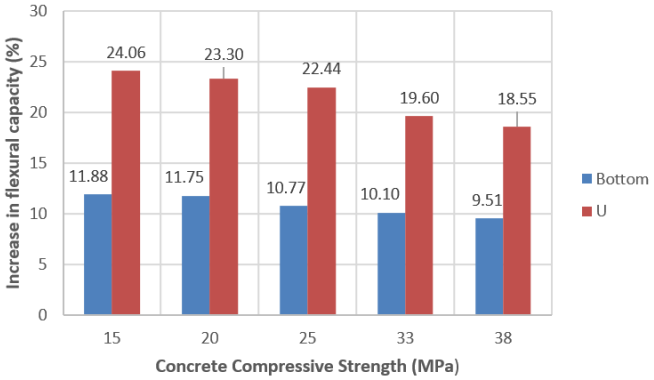

Figure 4.24 Increase percentage in flexural capacity with changing the concrete grade

4.4.4. Tensile Longitudinal Reinforcement Diameter

In this phase of the parametric study, the influence of the tensile reinforcement diameter on the flexural behavior of real scale RC beams strengthened with FRCC was evaluated. While the reference beam configuration utilized four 18 mm diameter bars as down side reinforcement (tension side), alternative configurations with 14 mm and 20 mm diameters were also considered to investigate their impact on overall structural performance.

For each case, the reinforcement ratio $\rho = As/Ac$ was computed, where As is the total area of the tensile reinforcement and Ac is the gross cross-sectional area of the concrete section. The Reinforcement ratio values are shown in table 4.5. Changes in the reinforcement diameter directly affect the moment capacity, stiffness, and ductility of the beam, especially under large deformation levels. These simulations help evaluate how sensitive the structural response is to variations in tensile reinforcement quantity, and to what extent the FRCC strengthening interacts with different levels of internal steel reinforcement.

Table 4.5 *reinforcement Ratio*

Rebar Diameter (mm)	Reinforcement Ratio (ρ)
14	0.41
18	0.68
20	0.84

By analysing the outcomes for beams strengthened using both bottom reinforcement and U-jacketing with each rebar size, this study provides insight into the synergy between internal and external reinforcement systems, guiding optimal rebar selection in strengthened full-scale elements.

Figure 4.25 presents the load–displacement response of full-scale RC beams with varying tensile reinforcement diameters (14 mm, 18 mm, and 20 mm), strengthened using either bottom FRCC reinforcement or U-jacketing techniques. For each reinforcement size, both the strengthened and corresponding unstrengthen bare beam configurations (indicated by dashed lines with a "B" in the legend) are included to facilitate a direct comparison of the impact of FRCC strengthening. This comparison is essential to quantify the true contribution of the strengthening system relative to the internal steel reinforcement level.

In the bottom reinforcement configuration (Figure 4.25a), the load–displacement curves clearly show that increasing the tensile rebar diameter enhances the peak load capacity. For example, the bare beam with 14 mm reinforcement (14B) fails at a significantly lower load compared to the 18B and 20B cases. When FRCC is applied as bottom reinforcement, all beams exhibit increased peak strength and improved post-peak ductility compared to their unstrengthen versions. However, the relative improvement is more pronounced for the 14 mm configuration, which shows a considerable increase in strength. This suggests that FRCC strengthening is particularly effective in compensating for low internal reinforcement, mitigating early cracking and premature yielding. Conversely, in the 20 mm configuration, the relative gain in load capacity is smaller, although ductility still improves. The post-peak behavior of the strengthened beams also becomes more gradual, indicating enhanced energy dissipation and crack bridging from the FRCC overlay.

The trend is even more evident in the U-jacketing configuration (Figure 4.25b). This technique outperforms bottom reinforcement in peak load for all reinforcement diameters. U-jacketed beams demonstrate not only higher load-carrying capacity but also a more stable and extended post-peak plateau, particularly in the 14 mm and 18 mm cases. The 20 mm U-jacketed beam achieves a load close to 410 kN with minimal degradation after peak, underlining the superior confinement and strain-hardening behavior provided by the U-jacketing scheme. Importantly, the dashed lines of the bare beams confirm that the greatest percentage increase due to strengthening is seen in the lightly reinforced (14 mm) case, again validating the effectiveness of FRCC in scenarios with deficient steel reinforcement.

The inclusion of bare beam curves also reveals another critical insight: as the internal reinforcement increases, the gap between strengthened and bare beam curves narrows, especially at higher load levels. This indicates a diminishing marginal benefit from FRCC strengthening when internal steel content is

already sufficient to resist flexural demands. However, across all cases, the FRCC layer still improves ductility and delays failure, suggesting that it enhances serviceability and safety even when strength gains are marginal.

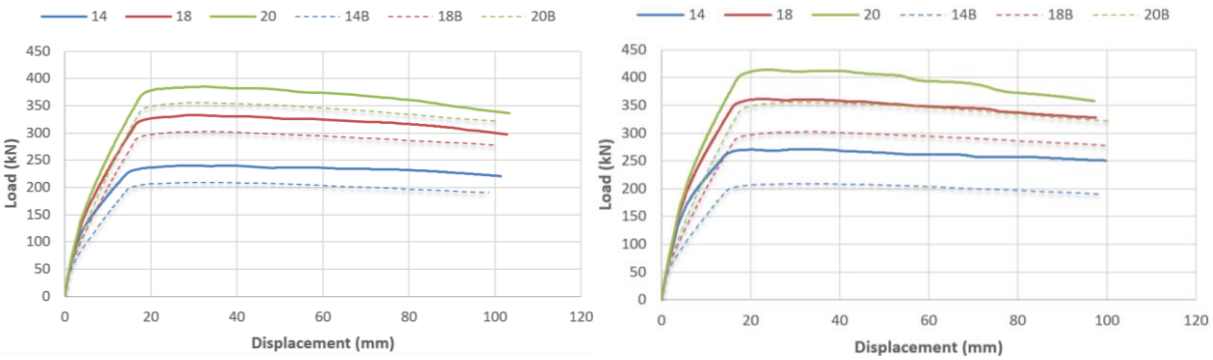

a) Bottom Reinforcement b) U-Jacketing

Figure 4.25 Load vs Displacement for distinct tensile rebars diameter

Figure 4.26 illustrates the percentage increase in flexural capacity of RC beams strengthened with FRCC-based bottom reinforcement and U-jacketing as a function of the tensile reinforcement ratio As/Ac, which varies with rebar diameter. The plotted data provides a direct quantitative measure of how internal steel reinforcement interacts with the applied FRCC strengthening and how this interaction evolves with increasing steel content. The reinforcement ratios of 0.41%, 0.68%, and 0.84% correspond respectively to tensile rebar diameters of 14 mm, 18 mm, and 20 mm, reflecting light, moderate, and high internal reinforcement conditions.

The chart shows a clear inverse relationship between the reinforcement ratio and the effectiveness of FRCC strengthening. For both bottom reinforcement and U-jacketing methods, the percentage increase in flexural capacity decreases as the reinforcement ratio increases. When the steel content is lowest (0.41%), bottom reinforcement yields a 15.11% gain, while U-jacketing achieves a significant 29.82% improvement. These results confirm that FRCC strengthening is most beneficial in beams with low internal reinforcement, where the external system can contribute substantially to the flexural resistance and stiffness. The added material enhances crack control, delays yielding, and significantly boosts the overall moment capacity.

As the reinforcement ratio increases to 0.68%, the efficiency of the strengthening methods declines. The bottom reinforcement method achieves a reduced gain of 10.10%, while U-jacketing still offers a respectable 19.60% improvement. This transition indicates that while FRCC strengthening continues to be effective, its relative contribution becomes less dominant as internal steel begins to take over more of the flexural load-carrying function.

At the highest reinforcement ratio of 0.84%, the trend continues, with bottom reinforcement producing only an 8.19% increase and U-jacketing a 16.45% increase. This behavior aligns with structural mechanics principles: as the internal steel reinforcement becomes more substantial, the beam becomes less reliant on external strengthening systems. Consequently, the marginal benefit from FRCC retrofitting diminishes, particularly for bottom reinforcement schemes that contribute primarily to tensile capacity without offering significant confinement or shear enhancement.

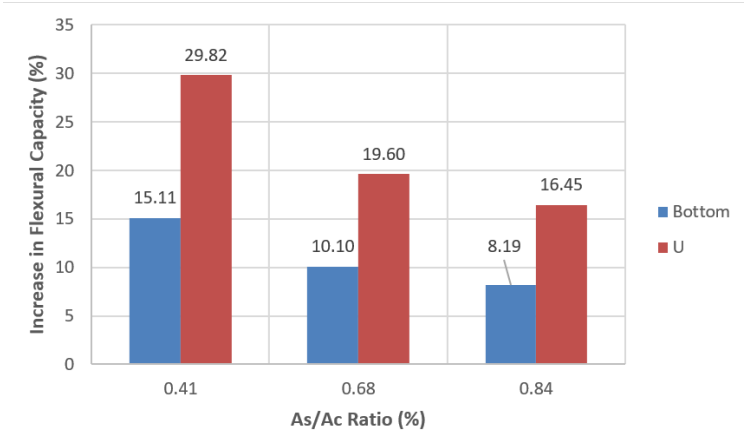

Figure 4.26 Increase percentage in flexural capacity with changing the tensile rebar diameter

5. DISCUSSION AND CONCLUSION

5.1. Discussion

5.1.1. FRCC 2.1% Tensile strength

As it was seen in experimental results and numerical modelling, based on different approaches, distinct values were obtained for the tensile strength of the FRCC2.1% material. There are various uncertainties affecting the result of all methods. As a results, the final value for tensile strength cannot be concluded, however, the result of each method can be discussed and compared. All the results are shown in table5.1.

Table 5.1 *FRCC 2.1% Tensile Strength*

Approach	Tensile Strength (MPa)
Material Characterrization	6
DIC Bottom Reinforcement	6.1
DIC U-Jacketeing	6.2
Beam Testing Bottom Reinforcement	8
Beam Testing U-Jacketing	8

The tensile strength obtained from material characterization is reported as 6 MPa, which serves as a baseline reference for the other methods. Values derived from DIC analysis during bottom reinforcement and U-jacketing beam tests are slightly higher, measured at 6.068 MPa and 6.232 MPa, respectively. This subtle increase suggests that in situ tensile performance, as captured during flexural testing, may reflect localized enhancements not fully captured in standard characterization procedures.

In contrast, the tensile strengths determined from the calibrated beam testing models for both strengthening configurations are reported as 8 MPa, marking the highest values among the group. This suggests that the global behavior observed in beam numerical simulations may require a higher tensile input to match experimental responses, likely accounting for additional mechanisms such as post-cracking behavior or composite action at the interface.

5.1.2. Effect of fiber ratio on Flexural behaviour

As it was seen previously, the RC beams strengthen with U-jacketing layer of FRCC material were experimentally and numerically investigated. As a result of beam numerical modelling calibration, the tensile strength of each material is obtained and shown in table5.2.

As it can be seen, the 1.1% fiber ratio exhibited 5.045MPa tensile strength and enhancing the steel fiber content to 2.0% leads to a substantial increase in tensile strength, achieving a peak value of 8 MPa. This outcome underscores the critical role of fiber volume in improving the tensile response, as the denser steel fiber network provides superior crack bridging capacity and post-cracking toughness.

Moreover, a hybrid composition incorporating 1.1% steel fiber and 1% polyethylene (PE) fiber also attains a tensile strength of 8 MPa, equivalent to the 2% steel fiber mix. This suggests that the hybrid system benefits from the complementary mechanical characteristics of the two fiber types, steel fibers effectively controlling wider cracks, while PE fibers contribute to controlling microcracks and enhancing strain hardening. Furthermore, the results highlight that both increasing the steel fiber content and adopting a hybrid reinforcement strategy are viable approaches for achieving high tensile performance in FRCC.

Table 5.2 *Variation in tensile strength based on distinct fiber ratios*

Approach	Tensile Strength (Mpa)
1.1% steel fiber	5
2.0% steel fiber	8
1.1% steel fiber +1% PE fiber	8

The load vs displacement curve shown in figure5.1 illustrates the experimental result of same materials. The beam with 2.00% steel fiber demonstrates the highest peak load, reaching approximately 61 kN, indicating superior initial stiffness and load-bearing capacity. This can be attributed to the high content of steel fibers, which significantly enhances the tensile resistance and bridging effect across cracks. Moreover, the post-peak behavior of this beam remains relatively stable, showing gradual load reduction with increasing displacement, which signifies improved ductility and energy absorption before failure.

In contrast, the 1.10% steel fiber mixture results in a lower peak load, around 54 kN, and exhibits a steeper drop post-peak, indicating reduced ductility and a more brittle failure mechanism. This behavior highlights the limitations of lower fiber content in providing sufficient crack control and tensile resistance under increasing deformation demands.

The 2.10% hybrid fiber mixture (combining steel and PE fibers) presents an intermediate peak load—slightly below the 2.00% steel fiber sample—but shows a remarkably extended displacement capacity, with sustained load resistance beyond 40 mm of displacement. This prolonged ductile response is a key advantage of hybrid fiber systems. While the peak strength is marginally compromised compared to pure steel fiber reinforcement, the synergy between steel and PE fibers greatly enhances crack distribution and strain-hardening behavior, allowing the structure to undergo significant deformation without abrupt strength loss.

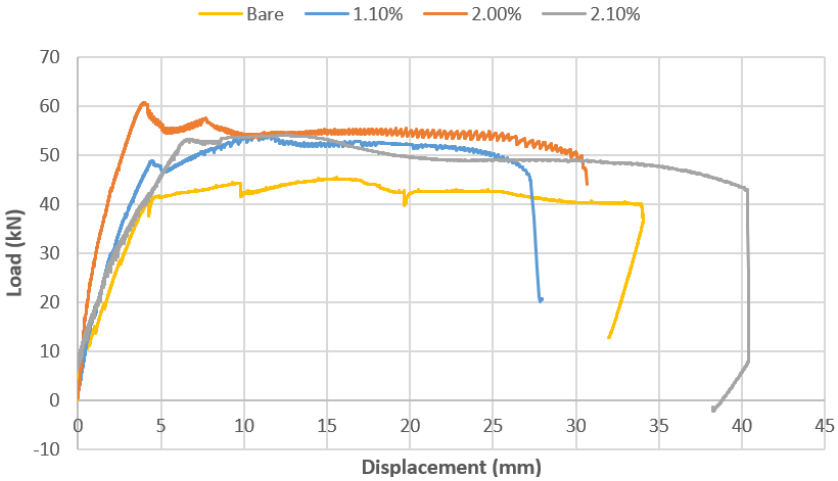

Figure 5.1 Load vs Displacement for distinct fiber ratios

The effect of fiber ratio on the flexural capacity of U-jacketing strengthened RC beams is presented in the figure5.2. At a fiber ratio of 1.1%, the flexural capacity increased by approximately 19% relative to the bare RC beam, indicating that even a modest amount of fibers can contribute to crack control and improved load resistance. The highest enhancement was achieved at a fiber ratio of 2%, where the flexural capacity reached an increase of about 34%, signifying that this dosage represents an optimal level at which fibers are well-dispersed and effectively engaged in bridging cracks and resisting tensile stresses. Conversely, a further increase to 2.1% resulted in a decline in performance, with the improvement reduced back to nearly 19%, comparable to the lowest tested ratio.

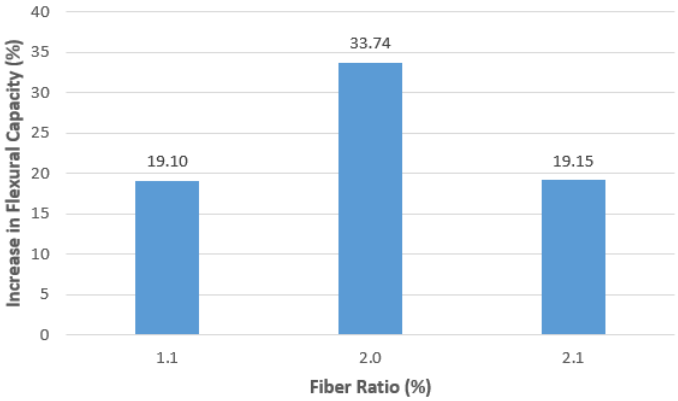

Figure 5.2 Load vs Displacement for distinct fiber ratios

5.1.3. Comparison with other flexural strengthening techniques

Finally, the results of all the beams that are tested in the experimental test campaign are shown in figure5.3. The graph presents the experimental load vs displacement behavior of six reinforced concrete (RC) beams under flexural loading. These include a bare beam (control specimen without external reinforcement), two beams strengthened using CFRP with NSM and EBR and three beams reinforced with FRCC at 1.1%, 2.0%, and 2.1% fiber volume fractions.

- Bare Beam Behavior

The bare beam exhibits a typical ductile response of an under-reinforced RC section, reaching a peak load of around 44 kN followed by a gradual reduction in load-carrying capacity. The load plateau and gradual softening signify yielding of reinforcement and subsequent crushing of concrete in compression.

- CFRP-Strengthened Beams: EBR and NSM

The beams strengthened using CFRP exhibit improved performance over the bare beam but vary based on the technique:
EBR enhances initial stiffness and the load capacity reaches around 42 kN, but shows brittle behavior with sudden drops in load after peak. The reinforcement likely delaminated or debonded, which is a common failure mode in EBR systems.
NSM demonstrates a significantly higher load capacity (peaking near 64 kN) and retains the load well after the initial peak. However, it experiences a sudden drop indicating brittle failure, possibly due to bond failure between the NSM rod and the concrete cover. Still, it provides superior strength enhancement compared to both EBR and the bare beam.

- Comparative Analysis

The bare RC beam exhibits the lowest ultimate load of approximately 45 kN with a displacement capacity around 34 mm, failing in a typical brittle manner with limited ductility. The EBR system shows a moderate decrease, reaching a peak load of about 40 kN but with lower displacement capacity (22 mm), suggesting premature debonding of externally bonded laminates as the governing failure mode. The NSM strengthening demonstrates a higher efficiency, achieving a maximum load of nearly 63 kN, corresponding to a ~43% increase over the bare beam. However, it failed abruptly at a relatively small displacement of 11 mm, indicating a brittle failure governed by debonding or rupture of the embedded reinforcement.

In contrast, the FRCC-strengthened beams displayed a more balanced performance. At a fiber ratio of 1.1%, the ultimate load increased to 52 kN (approximately 18% improvement over the bare specimen), though the displacement capacity remained close to that of the control. The beam with 2% fiber ratio exhibited the best performance, reaching a peak load of 60 kN, corresponding to a 34% increase, while also maintaining good post-peak ductility, reflecting the fibers' contribution to crack bridging and energy dissipation. Interestingly, at 2.1% fiber ratio, the load capacity was slightly lower (54 kN, 19% increase), but the displacement capacity extended to nearly 40 mm, the highest among all specimens. This indicates that the use of PE fibers, while not maximizing strength, improved deformability and post-peak energy absorption, suggesting a shift in the failure mode towards a more ductile response.

Overall, the comparison shows that while NSM produced the highest load capacity, it suffered from premature brittle failure. FRCC with 2% fibers offered the best balance between strength and ductility, whereas the 2.1% fiber ratio maximized displacement capacity, albeit at the cost of reduced peak strength. These findings emphasize the importance of optimizing fiber dosage to achieve desirable combinations of load capacity and ductility in strengthened RC beams.

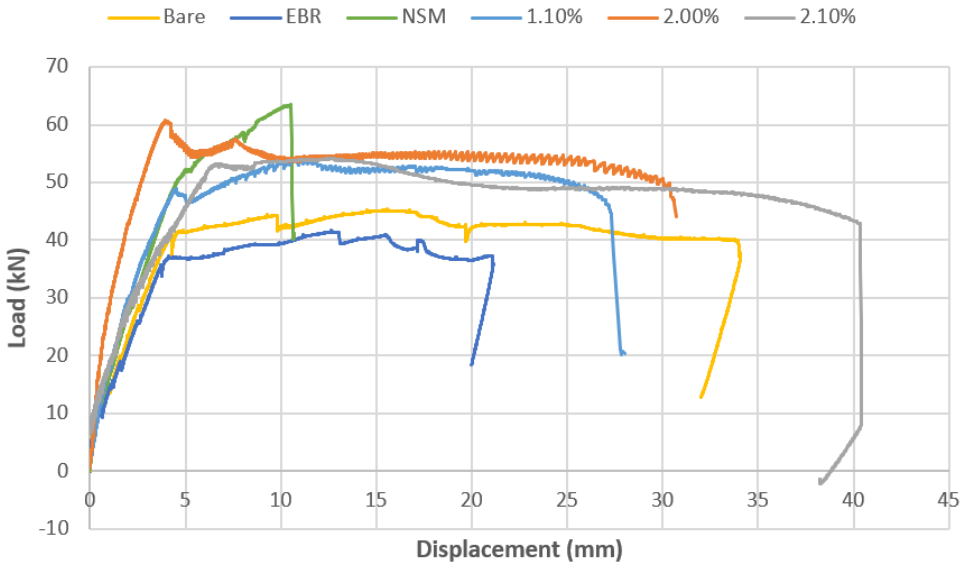

Figure 5.3 Experimental Load vs Displacement for all RC beams

5.2. Conclusion

The research explored the effectiveness of steel- and polyethylene-fiber-reinforced cementitious composites (FRCCs) as inorganic strengthening systems for RC beams, comparing bottom reinforcement and U-jacketing configurations through experimental, digital image correlation, and numerical modelling approaches. The key findings are:

- Both strengthening methods—bottom reinforcement and U-jacketing—significantly enhanced the flexural performance of RC beams compared to the bare RC beam. Bottom reinforcement increased peak flexural capacity by 10.1%, while U-jacketing achieved a higher improvement of about 19.6%.
- In comparison of 2 strengthening configurations, U-jacketing yields superior peak and post-peak behaviour and deformation capacity, promoting improved ductility and residual performance. The displacement capacity improved by nearly 8% for U jacketing in comparison to bottom reinforcement.
- The strain distribution patterns from DIC reveal that U-jacketing controls crack localization better, producing finer, more uniform cracks, whereas bottom reinforcement shows more pronounced localized cracking.
- The use of hybrid FRCC layers provides a balanced strengthening strategy. Energy absorption capacity increased by approximately 19% relative to the bare beam, highlighting improvements in toughness, energy dissipation, and serviceability without relying solely on increasing flexural strength.
- The reinforcement ratio of internal reinforcements affect the effectiveness of the FRCC strengthening significantly decreasing from almost 30% to 16% for U jacketing and from 15% to 8% for bottom reinforcement as the reinforcement ratio increases. Similarly, as the concrete grade raises, this effectiveness decreases. Varying from 24% to 18% for U jacketing and from almost 12% to 9% in bottom reinforcement.

5.3. Further Developments

While this study has demonstrated the potential of steel-FRCC systems for flexural strengthening of RC beams, several aspects remain open for future exploration and refinement. The following directions are recommended for further development:

- Shear Strengthening: This thesis focused primarily on flexural behavior. Future work should investigate the performance of FRCC strengthening for shear critical elements.
- Cyclic and Seismic Loading: Given the ductility and energy dissipation capacity of steel-FRCCs, additional experimental studies under cyclic and reversed loading would provide valuable insight into their effectiveness for seismic retrofitting.

- Full-scale Structural Testing: Expanding the current research to include full-scale structural components—such as slab-beam-column connections, bridge girders, or precast elements—would improve the practical applicability of the findings for real-world infrastructure retrofitting.
- Life-Cycle Assessment (LCA): Integrating environmental performance metrics through life-cycle cost and impact assessments can offer a holistic view of the sustainability benefits provided by using recycled steel fibers and inorganic matrices.
- Standardization and Design Guidelines: To facilitate broader adoption of FRCC systems in structural strengthening, the development of simplified design methodologies, standard detailing practices, and implementation protocols is needed.

REFERENCES

[1] A. O. Ates *et al.*, "Seismic retrofit of substandard RC columns using sprayed glass fiber-reinforced mortar and basalt textile reinforcement," *J. Earthq. Eng.*, vol. 28, no. 6, pp. 1615–1642, 2024.

[2] F. Sharifianjazi *et al.*, "Fibre-reinforced polymer reinforced concrete members under elevated temperatures: a review on structural performance," *Polymers (Basel).*, vol. 14, no. 3, p. 472, 2022.

[3] Y. Shao, W. Nguyen, M. J. Bandelt, C. P. Ostertag, and S. L. Billington, "Seismic performance of high-performance fiber-reinforced cement-based composite structural members: A review," *J. Struct. Eng.*, vol. 148, no. 10, p. 3122004, 2022.

[4] C. E. Chalioris, P.-M. K. Kosmidou, and C. G. Karayannis, "Cyclic response of steel fiber reinforced concrete slender beams: An experimental study," *Materials (Basel).*, vol. 12, no. 9, p. 1398, 2019.

[5] X. Li, C. Lu, Y. Cui, L. Zhou, and L. Zheng, "Bond behavior between high-strength rebar and steel-fiber-reinforced concrete under the influence of the fraction of steel fiber by volume and high temperature," *Appl. Sci.*, vol. 13, no. 4, p. 2399, 2023.

[6] J. Yang, Y. Zhang, and J. Huang, "The strengthening theory of steel fiber reinforced concrete and its application in tunnel engineering: A review," *J. Eng. Fiber. Fabr.*, vol. 19, p. 15589250241239242, 2024.

[7] A. Zhou, H. Wei, T. Liu, D. Zou, Y. Li, and R. Qin, "Interfacial technology for enhancement in steel fiber reinforced cementitious composite from nano to macroscale," *Nanotechnol. Rev.*, vol. 10, no. 1, pp. 636–652, 2021.

[8] M. Y. Alkhateeb and F. Hejazi, "Strengthening reinforced concrete beams through integration of cfrp bars, mechanical anchorage system, and concrete jacketing," *Materials (Basel).*, vol. 17, no. 12, p. 2794, 2024.

[9] K. Flores Ferreira, M. C. Rampini, G. Zani, M. Colombo, and M. di Prisco, "Experimental investigation on the use of Fabric-Reinforced Cementitious Mortars for the retrofitting of reinforced concrete dapped-end beams," *Struct. Concr.*, vol. 24, no. 4, pp. 4577–4605, 2023.

[10] C. E. Chalioris, A. G. Zapris, and C. G. Karayannis, "U-jacketing applications of fiber-reinforced polymers in reinforced concrete T-beams against shear—Tests and design," *Fibers*, vol. 8, no. 2, p. 13, 2020.

[11] X. Shen, W. Chen, B. Li, C. M. Hancock, and Y. Xu, "Flexural strengthening of reinforced concrete beams using fabric reinforced alkali-activated slag matrix," *J. Build. Eng.*, vol. 33, p. 101865,

2021.

[12] B. Gunes, T. Cosgun, B. Sayin, and A. Mangir, "Seismic performance of an existing low-rise RC building considering the addition of a new storey," *Rev. la Construcción*, vol. 18, no. 3, pp. 459–475, 2019.

[13] A. D'Ambrisi and F. Focacci, "Flexural strengthening of RC beams with cement-based composites," *J. Compos. Constr.*, vol. 15, no. 5, pp. 707–720, 2011.

[14] A. A. Torres-Acosta, S. Navarro-Gutierrez, and J. Terán-Guillén, "Residual flexure capacity of corroded reinforced concrete beams," *Eng. Struct.*, vol. 29, no. 6, pp. 1145–1152, 2007.

[15] Y. Wang and J. Wu, "Flexural behavior of corroded concrete beams strengthened with carbon fiber-reinforced polymer," *Materials (Basel).*, vol. 16, no. 12, p. 4355, 2023.

[16] X. Li, H.-L. Lv, G.-C. Zhang, S.-Y. Sha, and S.-C. Zhou, "Seismic retrofitting of rectangular reinforced concrete columns using fiber composites for enhanced flexural strength," *J. Reinf. Plast. Compos.*, vol. 32, no. 9, pp. 619–630, 2013.

[17] S. A. Scala, M. T. De Risi, and G. M. Verderame, "Code-based brittle capacity models for seismic assessment of pre-code RC buildings: comparison and consequences on retrofit," *Bull. Earthq. Eng.*, vol. 22, no. 13, pp. 6643–6674, 2024.

[18] S. S. Abdulhameed, E. Wu, and B. Ji, "Mechanical prestressing system for strengthening reinforced concrete members with prestressed carbon-fiber-reinforced polymer sheets," *J. Perform. Constr. Facil.*, vol. 29, no. 3, p. 4014081, 2015.

[19] R. El Ghadioui, J. Wagner, J. Klein, T. Proske, M. Curbach, and C. Graubner, "RC members with a flexural-strengthening layer of CFRP textile-reinforced concrete under monotonic and cyclic long-term loading," *Struct. Concr.*, vol. 23, no. 2, pp. 939–953, 2022.

[20] J. Esmaeili, O. R. Aghdam, K. Andalibi, J. Kasaei, and O. Gencel, "Experimental and numerical investigations on a novel plate anchorage system to solve FRP debonding problem in the strengthened RC beams," *J. Build. Eng.*, vol. 45, p. 103413, 2022.

[21] F. Ceroni, M. Pecce, S. Matthys, and L. Taerwe, "Debonding strength and anchorage devices for reinforced concrete elements strengthened with FRP sheets," *Compos. Part B Eng.*, vol. 39, no. 3, pp. 429–441, 2008.

[22] G. M. Calvi, G. Magenes, and S. Pampanin, "Relevance of beam-column joint damage and collapse in RC frame assessment," *J. Earthq. Eng.*, vol. 6, no. spec01, pp. 75–100, 2002.

[23] B. Tejedor, E. Lucchi, D. Bienvenido-Huertas, and I. Nardi, "Non-destructive techniques (NDT) for the diagnosis of heritage buildings: Traditional procedures and futures perspectives," *Energy*

Build., vol. 263, p. 112029, 2022.

[24] G. Campione, M. Fossetti, C. Giacchino, and G. Minafò, "RC columns externally strengthened with RC jackets," *Mater. Struct.*, vol. 47, no. 10, pp. 1715–1728, 2014.

[25] M. R. Maheri and A. Sahebi, "Use of steel bracing in reinforced concrete frames," *Eng. Struct.*, vol. 19, no. 12, pp. 1018–1024, 1997.

[26] P. D. Gkournelos, T. C. Triantafillou, and D. A. Bournas, "Seismic upgrading of existing reinforced concrete buildings: A state-of-the-art review," *Eng. Struct.*, vol. 240, p. 112273, 2021.

[27] G. Minafò, F. Di Trapani, and G. Amato, "Strength and ductility of RC jacketed columns: A simplified analytical method," *Eng. Struct.*, vol. 122, pp. 184–195, 2016.

[28] S. Raza, M. K. I. Khan, S. J. Menegon, H.-H. Tsang, and J. L. Wilson, "Strengthening and repair of reinforced concrete columns by jacketing: State-of-the-art review," *Sustainability*, vol. 11, no. 11, p. 3208, 2019.

[29] G. Terenzi, E. Fuso, S. Sorace, and I. Costoli, "Enhanced seismic retrofit of a reinforced concrete building of architectural interest," *Buildings*, vol. 10, no. 11, p. 211, 2020.

[30] M. Z. Naser, R. A. Hawileh, and J. A. Abdalla, "Fiber-reinforced polymer composites in strengthening reinforced concrete structures: A critical review," *Eng. Struct.*, vol. 198, p. 109542, 2019.

[31] Z. Wang *et al.*, "Long-term durability of basalt-and glass-fibre reinforced polymer (BFRP/GFRP) bars in seawater and sea sand concrete environment," *Constr. Build. Mater.*, vol. 139, pp. 467–489, 2017.

[32] R. Guo, C. Li, Y. Niu, and G. Xian, "The fatigue performances of carbon fiber reinforced polymer composites–a review," *J. Mater. Res. Technol.*, vol. 21, pp. 4773–4789, 2022.

[33] R. K. S. Raman, F. Guo, S. Al-Saadi, X.-L. Zhao, and R. Jones, "Understanding fibre-matrix degradation of FRP composites for advanced civil engineering applications: an overview," *Corros. Mater. Degrad.*, vol. 1, no. 1, pp. 27–41, 2018.

[34] H. Gonabadi, A. Oila, A. Yadav, and S. Bull, "Investigation of anisotropy effects in glass fibre reinforced polymer composites on tensile and shear properties using full field strain measurement and finite element multi-scale techniques," *J. Compos. Mater.*, vol. 56, no. 3, pp. 507–524, 2022.

[35] Y. O. Özkılıç, E. Madenci, and L. Gemi, "Tensile and compressive behaviors of the pultruded GFRP lamina," *Turkish J. Eng.*, vol. 4, no. 4, pp. 169–175, 2020.

[36] C. Mazzotti and M. Savoia, "FRP-concrete bond behaviour under cyclic debonding force," *Adv. Struct. Eng.*, vol. 12, no. 6, pp. 771–780, 2009.

[37] A. Bilotta, F. Ceroni, M. Di Ludovico, E. Nigro, M. Pecce, and G. Manfredi, "Bond efficiency of EBR and NSM FRP systems for strengthening concrete members," *J. Compos. Constr.*, vol. 15, no. 5, pp. 757–772, 2011.

[38] V. C. Li, "On engineered cementitious composites (ECC) a review of the material and its applications," *J. Adv. Concr. Technol.*, vol. 1, no. 3, pp. 215–230, 2003.

[39] B. A. Graybeal, "Material property characterization of ultra-high performance concrete," United States. Department of Transportation. Federal Highway Administration ..., 2006.

[40] M. R. Islam, L. Bin Bashar, D. K. Saha, and N. Rafi, "Comparison and selection of airfoils for small wind turbine between NACA and NREL's S series airfoil families," *Int. J. Res. Electr. Electron. Commun. Eng.*, vol. 4, no. 2, pp. 1–11, 2019.

[41] A. Bentur and S. Mindess, *Fibre reinforced cementitious composites*. CRC press, 2006.

[42] Z. Lin, T. Kanda, and V. C. Li, "On interface property characterization and performance of fiber reinforced cementitious composites," 1999.

[43] V. C. Li, "From micromechanics to structural engineering-the design of cementitous composites for civil engineering applications," 1993.

[44] V. C. Li, "Engineered cementitious composites (ECC) material, structural, and durability performance," 2008.

[45] E. Parant, R. Pierre, and F. Le Maou, "Durability of a multiscale fibre reinforced cement composite in aggressive environment under service load," *Cem. Concr. Res.*, vol. 37, no. 7, pp. 1106–1114, 2007.

[46] L. Bertolini, B. Elsener, P. Pedeferri, E. Redaelli, and R. B. Polder, *Corrosion of steel in concrete: prevention, diagnosis, repair*. John Wiley & Sons, 2013.

[47] F. Ossio, C. Salinas, and H. Hernández, "Circular economy in the built environment: A systematic literature review and definition of the circular construction concept," *J. Clean. Prod.*, vol. 414, p. 137738, 2023.

[48] X. Qin, X. Huang, Y. Li, and S. Kaewunruen, "Sustainable design framework for enhancing shear capacity in beams using recycled steel fiber-reinforced high-strength concrete," *Constr. Build. Mater.*, vol. 411, p. 134509, 2024.

[49] A. Michalik, F. Chyliński, J. Bobrowicz, and W. Pichór, "Effectiveness of concrete reinforcement with recycled tyre steel fibres," *Materials (Basel).*, vol. 15, no. 7, p. 2444, 2022.

[50] F. Mu, L. Huo, X. Yang, W. Zhao, F. Li, and Q. Gui, "Mechanical Properties of Sprayed FRCC Reinforced RC Beams With/Without Precast Cracks and DIC-Based Crack Identification,"

Buildings, vol. 15, no. 6, p. 908, 2025.

[51] V. C. Li and C. K. Y. Leung, "Steady-state and multiple cracking of short random fiber composites," *J. Eng. Mech.*, vol. 118, no. 11, pp. 2246–2264, 1992.

[52] H. QIAN, C. CHEN, Q. ZHANG, L. KANG, and J. ZHAO, "Experimental study on flexural behavior of RC beam strengthened with self-repairing SMA/ECC composites materials," *Eng. Mech.*, vol. 40, no. 6, pp. 73–84, 2023.

[53] A. T. Atmajayanti, Y. Haryanto, F.-P. Hsiao, H.-T. Hu, and L. Nugroho, "Effective Flexural Strengthening of Reinforced Concrete T-Beams Using Bonded Fiber-Core Steel Wire Ropes," *Fibers*, vol. 13, no. 5, p. 53, 2025.

[54] N. Khattak, M. Mansour, T. El-Maaddawy, and N. Ismail, "Continuous reinforced concrete beams strengthened with fabric-reinforced cementitious matrix: experimental investigation and numerical simulation," *Buildings*, vol. 12, no. 1, p. 27, 2021.

[55] J. Tian *et al.*, "Experimental study and analysis model of flexural synergistic effect of reinforced concrete beams strengthened with ECC," *Constr. Build. Mater.*, vol. 352, p. 128987, 2022.

[56] C. R. Siva and A. Pankaj, "Flexural behavior of reinforced concrete beams with high performance fiber reinforced cementitious composites," *J. Cent. South Univ.*, vol. 26, no. 9, pp. 2609–2622, 2019.

[57] M. Wasef, A. Hassan, and N. M. Kassem, "Flexural Behaviour of Reinforced Concrete Beams Strengthened with Textile-Reinforced Strain Hardening Geopolymer Composites (TR-SHGC)," *Int. J. Concr. Struct. Mater.*, vol. 19, no. 1, p. 38, 2025.

[58] A. T. Baraghith, A.-H. A. Khalil, E. E. Etman, and R. N. Behiry, "Improving the shear behavior of RC dapped-end beams using precast strain-hardening cementitious composite (P-SHCC) plates," in *Structures*, Elsevier, 2023, pp. 978–997.

[59] A. Mandor and A. El Refai, "Strengthening the hogging and sagging regions in continuous beams with fiber-reinforced cementitious matrix (FRCM): Experimental and analytical investigations," *Constr. Build. Mater.*, vol. 321, p. 126341, 2022.

[60] H. Liu, J. Xiao, and T. Ding, "Flexural performance of 3D-printed composite beams with ECC and recycled fine aggregate concrete: Experimental and numerical analysis," *Eng. Struct.*, vol. 283, p. 115865, 2023.

[61] M. Bai, J. Xiao, Y. Wu, and T. Ding, "Experimental and numerical study on the flexural behavior of 3D-printed composite beams with U-shaped ECC formwork," *Eng. Struct.*, vol. 312, p. 118225, 2024.

[62] L. Facconi, G. Plizzari, and F. Minelli, "Elevated slabs made of hybrid reinforced concrete: Proposal of a new design approach in flexure," *Struct. Concr.*, vol. 20, no. 1, pp. 52–67, 2019.